Informed Random Partition Models with Temporal Dependence

Sally Paganin

Department of Statistics, The Ohio State University, Columbus, Ohio

and Garritt L. Page

Department of Statistics, Brigham Young University, Provo, Utah

and Fernando Andrés Quintana, Departamento de Estadística

Pontificia Universidad Católica de Chile, Santiago

November, 2023

Abstract

Model-based clustering is a powerful tool that is often used to discover hidden structure in data by grouping observational units that exhibit similar response values. Recently, clustering methods have been developed that permit incorporating an "initial" partition informed by expert opinion. Then, using some similarity criteria, partitions different from the initial one are down weighted, i.e. they are assigned reduced probabilities. These methods represent an exciting new direction of method development in clustering techniques. We add to this literature a method that very flexibly permits assigning varying levels of uncertainty to any subset of the partition. This is particularly useful in practice as there is rarely clear prior information with regards to the entire partition. Our approach is not based on partition penalties but considers individual allocation probabilities for each unit (e.g., locally weighted prior information). We illustrate the gains in prior specification flexibility via simulation studies and an application to a dataset concerning spatio-temporal evolution of PM_{10} measurements in Germany.

1 Introduction

Cluster analysis or unsupervised learning has become a popular tool to discover latent data structures. Several approaches that implement cluster analysis have emerged. One is purely algorithmic, based on assigning individuals/units to groups based on a distance metric (e.g., k-means or hierarchical clustering). A second one incorporates probabilistic group assignment by way of a finite/infinite mixture model. From a Bayesian perspective using finite or infinite mixtures to carry out clustering has received considerable attention in the statistical literature. A prototypical application of this strategy involves the adoption of a model that can be expressed as the convolution of a continuous kernel $k(y \mid \theta)$ and a discrete random probability measure G that can be represented as $G(\cdot) = \sum_{h=1}^{H} w_h \delta_{\theta_h}$ with $1 < H \leq \infty$. Here, $\theta_1, \ldots, \theta_H$ are i.i.d. from some distribution G_0 supported on a suitable space Θ, and that are independent of the weights $\{w_h\}$, which are required to be a.s. non-negative and to satisfy $\Pr(\sum_{h=1}^{H} w_h = 1) = 1$. The mixture model that so arises adopts the form $p(y \mid \{w_h\}, \{\theta_h\}) = \int_{\Theta} k(y \mid \theta) \, dG(\theta) = \sum_{h=1}^{H} w_h k(y \mid \theta_h)$. Models based on such constructed mixtures have become quite popular in the Bayesian clustering literature, as mixture components are used to define different subsets in a partition. Under this approach, distributions on partitions are *induced* from the (in)finite mixture model. Some recent applications are given in Ni et al. (2020), Lijoi et al. (2023) and references therein. For recent reviews in Bayesian cluster analysis, see Wade (2023) and Grazian (2023).

A third Bayesian approach consists of modeling the partitioning of units into groups directly by way of a random partition model (Müller et al. 2015). This procedure allows the user much tighter control on prior co-clustering probabilities compared to the case where

the induced partition model is employed. This added control has been shown to provide great benefit in, for example, the temporal evolution of random partition distributions when a sequence of partitions is available (a case we consider here); see a discussion of this in Page et al. (2022). Apart from being seemingly more coherent (i.e., the object of inferential inference is that which receives modeling attention), Bayesian random partition models allow practitioners to more directly include prior information in the clustering. An early example of this type of modeling is the product partition model (PPM), described in Hartigan (1990). This model can be specified in a way that its random partition distribution coincides with the well known clustering properties arising from the popular Dirichlet process (DP) of Ferguson (1973). The PPMx, discussed in Müller et al. (2011a) is a modification of the PPM to include covariate dependence in the prior partition distribution, in a way similar to nonparametric regression. The modification is driven by cohesion functions that encourage homogeneity of subsets in terms of covariate values. A related construction appears in Park and Dunson (2010). Argiento et al. (2022) extended the PPMx to clustering distributions that arise from normalized completely random measures (Regazzini et al.; 2003). Other options of random partition models include the Ewens-Pitman attraction approach by Dahl et al. (2017), where pairwise similarities are used to specify cluster allocations. Franzolini et al. (2023) introduce the class of telescopic clustering models, based on the notion of conditional partial exchangeability, that allows for dependence among partitions of a given set of subjects but based on different features, which is particularly suitable for multi-view or longitudinal data.

Recently, Smith and Allenby (2020) and Paganin et al. (2021) developed for the first time methods that permit users to inform the prior "location" on the partition space, by including an initial guess on what the clustering might be. In this work, we propose an alternative approach to define an *informed partition model*, that is, a model that can accommodate available prior information on a given partition. In particular, we build on ideas in Page

3

et al. (2022), who developed a flexible joint probability model for a sequence of temporally correlated partitions. We extend their method to include the notion of an "initial" partition that informs the clustering but whose impact can either decay or persist through time. As a result our approach is from a completely different perspective compared to Smith and Allenby (2020) and Paganin et al. (2021) which results in a number of novel innovations. Paganin et al. (2021) explores the idea of adjusting partition probabilities based on the distance from the initial partition as defined by some loss function (they employ the variation of information loss by Meilă (2007)). This approach is available for any random partition distribution, but results in needing to evaluate a normalizing constant that becomes intractable even for relatively small sample sizes. In addition it is not possible to customize prior uncertainty for subsets of the initial partition. Smith and Allenby (2020) instead measure proximity to the initial partition by enumerating units that are co-clustered in the estimated partition and in the initial partition. Their development only considers a particular random partition distribution and depends on the order in which units are allocated. This approach too is not able to treat subsets of the initial partition with more uncertainty than others. Dahl, Warr and Jensen (2021)'s approach generalizes that of Smith and Allenby (2020) so that any random partition model can be employed and introduces a permutation parameter that removes dependence on order. They do consider varying degrees of initial partition uncertainty but only at the cluster level. Our approach accommodates any random partition model, does not depend on the order in which units are clustered, and scales relatively well. An additional key contribution we make is that our approach permits eliciting prior uncertainty at the unit level. The appeal of this property stems from the desire to flexibly express varying degrees of information certainty on various subsets of the initial partition. Informing the clustering of each unit individually allows us to put more prior weight on the co-clustering of a given subset of units compared to others for which less information is available. Lastly, our approach facilitates incorporating the initial partition information for a sequence of temporally

evolving partitions. Furthermore, spatially informed initial partitions are easily included in the proposed framework, thus allowing for a spatio-temporal modeling approach.

The rest of this article is organized as follows. Section 2 describes the general model for a single informed partition and its extension to a sequences of partitions that evolve in time. Some properties and special cases of interest are also stated and discussed. Section 3 describes and summarizes the results of extensive simulation studies carried out to explore various model aspects including how the prior distribution is specified, the effect of prior information on the temporal progression, and a comparison with alternative approaches to reflect prior information on partitions. Section 4 describes the results of applying the proposed approach to a sequence of particulate matter measurements over a number of time periods in Germany, where the relative strengths of various potential model specifications are assessed, especially, regarding the role of prior spatial information. Finally, Section 5 concludes with a summary and some additional considerations regarding model construction and performance.

2 The Model and Some Properties

In this section we first provide details of our method in the context of a single partition. Then we extend ideas to the case of a sequence of partitions and highlight various ways in which the initial partition can inform clustering.

2.1 Informed Partition for a Single Partition

We begin by introducing notation and basic ideas from methods described in Page et al. (2022), focusing on the special case where we observe one partition conditionally on a prior guess. We review this material to the extent required to present our own contribution. For any integer $m \geq 1$, let $[m] = \{1, \ldots, m\}$ and let $\rho = (S_1, \ldots, S_k)$ denote a partition of

$[m]$ where k is number of clusters and $S_1, \ldots, S_k$ the corresponding nonempty and mutually exclusive subsets of $[m]$ comprising ρ. Alternatively, ρ can be specified through the cluster membership indicators $c_1, \ldots, c_m$ such that $c_i = j \Leftrightarrow i \in S_j$. We will use $\rho_0 = (S_{01}, \ldots, S_{0k_0})$ to denote a user supplied initial partition and $c_{01}, \ldots, c_{0m}$ the corresponding cluster labels.

We construct a random probability model by specifying a prior distribution on ρ that accounts for the information contained in ρ_0, i.e. we specify a model of the form $\Pr(\rho \mid \rho_0)$. Following Page et al. (2022) we do so by introducing a set of auxiliary variables $\boldsymbol{\gamma} = (\gamma_1, \ldots, \gamma_m)$ that determines which units are allowed to be reallocated in ρ with respect ρ_0. Specifically, we introduce a collection of binary variables $\{\gamma_i : i = 1, \ldots, m\}$ as follows:

$$\gamma_i = \begin{cases} 1 & \text{if unit } i \text{ is } not \ to \ be \text{ reallocated with respect to } \rho_0 \\ 0 & \text{otherwise.} \end{cases} \tag{1}$$

We assume that $\gamma_i \overset{ind}{\sim} \text{Bern}(\alpha_i)$, $i = 1, \ldots, m$, with α_i controlling the probability that each unit follows the initial partition. In other words, values of α_i will reflect the prior beliefs in the initial guess, allowing for different degrees of uncertainty among observations. These prior beliefs can be included through the selection of a_i and b_i in $\alpha_i \sim \text{Beta}(a_i, b_i)$ which affords quite a bit of flexibility to the user. Indeed, varying degrees of confidence on the strength of those subsets contained in ρ_0 can be expressed under this general framework. To illustrate this point, consider the simple case of clustering six units based on the initial partition $\rho_0 = \{\{1, 3\}, \{2, 4, 5\}, \{6\}\}$. Further suppose that an expert is quite certain that units 1 and 3 should be grouped together and not grouped with unit 6, but less sure about units 2, 4, and 5. A straightforward way to account for this information is by setting $a_1 = a_3 = a_6 = 99$ and $b_1 = b_3 = b_6 = 1$ along with $a_2 = a_4 = a_5 = 1$ and $b_2 = b_4 = b_5 = 9$.

The conditional prior for the partition ρ takes the following form

$$\Pr(\rho \mid \rho_0) = \sum_{\gamma \in \Gamma} \Pr(\rho \mid \rho_0, \gamma) \Pr(\gamma), \tag{2}$$

where Γ denotes the collection of all possible vectors of zeros and ones of size m, and

$$\Pr(\gamma) = \prod_{i=1}^{m} \alpha_i^{\gamma_i} (1 - \alpha_i)^{1 - \gamma_i}. \tag{3}$$

The partition probability $\Pr(\rho = \lambda \mid \rho_0, \gamma)$ relies on the definition of *compatibility* introduced in Page et al. (2022), as discussed next. We say that partition ρ and ρ_0 are compatible with respect to γ, if ρ can be obtained from ρ_0 by reallocating items as indicated by γ, i.e., those items i such that $\gamma_i = 0$ for $i = 1, \ldots, m$. To check if ρ and ρ_0 are compatible with respect to γ we reason as follows. Let $\mathfrak{R} = \{i : \gamma_i = 1\}$ be the collection of units that are fixed according to the initial partition ρ_0 and let $\mathfrak{R}^C = \{i : \gamma_i = 0\}$ be the collection of units that are not. Denote by $\rho^{\mathfrak{R}}$ the "reduced" partition that remains after removing all items in $\mathfrak{R}$ from the subsets of ρ. Similarly, let $\rho_0^{\mathfrak{R}}$ be the reduced initial partition. Then ρ and ρ_0 are *compatible with respect to γ* if and only if $\rho_0^{\mathfrak{R}} = \rho^{\mathfrak{R}}$.

Let $\mathcal{P}$ denote the set of all partitions of m units and let $P_C(\rho_0, \gamma) = \{\rho \in \mathcal{P} : \rho_0^{\mathfrak{R}} = \rho^{\mathfrak{R}}\}$ be the collection of partitions that are compatible with ρ_0 based on γ. The conditional distribution $\Pr(\rho \mid \rho_0, \gamma)$ is a random partition distribution with support $P_C(\rho_0, \gamma)$, so that

$$\Pr(\rho = \lambda \mid \rho_0, \gamma) = \frac{\Pr(\rho = \lambda) \mathbb{I}\{\lambda \in P_C(\rho_0, \gamma)\}}{\sum_{\lambda' \in \mathcal{P}} \Pr(\rho = \lambda') \mathbb{I}\{\lambda' \in P_C(\rho_0, \gamma)\}}, \tag{4}$$

where $\Pr(\rho = \lambda)$ is an exchangeable partition probability function (EPPF; see, e.g. Pitman; 1995). Notice that if $\alpha_i = 1, \forall i$, then $\Pr(\rho \mid \rho_0) = \delta_{\rho_0}$, the prior collapses on the prior partition ρ_0, while $\alpha_i = 0, \forall i$, then $\Pr(\rho \mid \rho_0) = \Pr(\rho)$, the prior reduces to the chosen EPPF, i.e., ρ_0 plays no role in the prior specification. We will use the notation $\rho \sim iCRP(\rho_0, \alpha, M)$

to denote the special case in which ρ is distributed according to an informed partition model with $\Pr(\rho)$ in (4) corresponding to a Chinese Restaurant Process (CRP) prior as defined below (see Pitman; 1996, for a discussion on this name) and stated here for later reference:

$$\Pr(\rho = \{S_1, \ldots, S_k\} \mid M) = \frac{M^k}{\prod_{i=1}^n (M + i - 1)} \prod_{i=1}^k (|S_i| - 1)! \tag{5}$$

2.2 Informed partition model for a sequence of random partitions

Consider now a sequence of partitions $\boldsymbol{\rho} = (\rho_1, \ldots, \rho_T)$ of $[m]$ where $\rho_t = \{S_{t1}, \ldots, S_{tk_t}\}$ (alternatively cluster labels can be employed so that $c_{ti} = j$ implies that unit i is allocated to S_{tj}). Based on ideas in Page et al. (2022) we construct a prior model $p(\rho_1, \ldots, \rho_T \mid \rho_0)$ that potentially incorporates serial dependence among random partitions and is informed by ρ_0. Our construction extends the idea underlying (2) by introducing a matching $(T \times m)$-dimensional sequence of binary indicators $\boldsymbol{\gamma}$ where for $t = 1, \ldots, T$ and $i = 1, \ldots, m$, such that $\gamma_{ti} \sim \text{Bern}(\alpha_{ti})$ with $\alpha_{ti} \sim \text{Beta}(a_{ti}, b_{ti})$ and $\gamma_{ti} = 1$ if unit i is not to be reallocated when moving from time t to time $t + 1$, and $\gamma_{ti} = 0$ if it is up for possible reassignment. There is substantial flexibility in specifying $p(\boldsymbol{\rho} \mid \rho_0)$, which is why specific constructions are typically case-dependent. We discuss first the evolution of partitions, mentioning a couple of potentially useful alternatives:

Conditionally independence. In this case, we model the partitions in $\boldsymbol{\rho}$ as

$$p(\boldsymbol{\rho} \mid \rho_0) = p(\rho_1 \mid \rho_0) \times \cdots \times p(\rho_T \mid \rho_0),$$

that is, partitions are conditionally independent given the initial ρ_0, and where each of $p(\rho_t \mid \rho_0)$ is specified as in (2). A convenient default choice is to assume $\rho_t \sim iCRP(\rho_0, \boldsymbol{\alpha}_t, M)$, as defined in Section 2.1. This case is useful when it is judged that there is no time trend in the ρ_i's so that the influence of ρ_0 is constant across time.

Depending on the prior specifications for the $(T \times m)$-dimensional parameter $\boldsymbol{\alpha}$ we could have a model that includes a conditional i.i.d. specification (e.g. $a_{ti} = a_i$ and $b_{ti} = b_i$ for all t) or varying degrees of shrinkage towards ρ_0, e.g. as implied by a sequence of prior mean values $a_{ti}/(a_{ti} + b_{ti})$ that decrease with t for every i.

Markovian dependence. In this case, we follow Page et al. (2022) and consider a Markovian structure of the form

$$p(\boldsymbol{\rho} \mid \rho_0) = p(\rho_1 \mid \rho_0)p(\rho_2 \mid \rho_1) \cdots p(\rho_T \mid \rho_{T-1}), \tag{6}$$

where time dependence in the sequence of partitions is accounted for by using the partition at time $t - 1$ as the center to inform that at time t. A default choice here would be to specify $\rho_t \mid \rho_{t-1} \sim iCRP(\rho_{t-1}, \boldsymbol{\alpha}_t, M)$, that is, centering is done on the partition from the previous time, and where $\rho_1 \sim iCRP(\rho_0, \boldsymbol{\alpha}_1, M)$. This creates a Markovian structure for the sequence of partitions, that teamed with the flexibility inherent to the definition of the $\boldsymbol{\alpha}$ parameters (see the discussion below), facilitates propagating various degrees of dependence on the partition information supplied by ρ_0.

As previously observed, many particular definitions in this flexible model for the sequence of partitions are necessarily case-dependent. As a reasonable default choice, we suggest adopting (6).

We next discuss models for $\boldsymbol{\alpha}$. Generally speaking any possible specification will necessarily depend on the desired type of borrowing-of-strength. In what follows we consider by default the models described in Table 1, with the understanding that many more options are available, as required by specific prior features the user wishes to impose. As mentioned, the unit local and time×unit local models permit users to emphasize (or deemphasize) subsets of the initial partition. For instance, the Markovian model (6) with global $\boldsymbol{\alpha}$ and an empty ρ_0

Table 1: Possible priors for $\boldsymbol{\alpha}$

name	description: $\boldsymbol{\alpha} = (\alpha_{ti})$	model	borrowing-of-strength
global	$\alpha_{ti} = \alpha$, constant in i, t	$\alpha \sim \mathrm{Beta}(a, b)$	across time and units
time local	$\alpha_{ti} = \alpha_t$, constant in i	$\alpha_t \sim \mathrm{Beta}(a_t, b_t)$	across units
unit local	$\alpha_{ti} = \alpha_i$, constant in t	$\alpha_i \sim \mathrm{Beta}(a_i, b_i)$	across time
time$\times$unit local	unrestricted	$\alpha_{ti} \sim \mathrm{Beta}(a_{ti}, b_{ti})$	none

(i.e. a non-informed model) has the property that every ρ_t has a CRP marginal distribution, as shown in Page et al. (2022). Generally speaking, large values of $a_{ti}/(a_{ti} + b_{ti})$ will produce a prior that heavily concentrates on ρ_0 through time, while low values for $a_{ti}/(a_{ti} + b_{ti})$ will tend to induce near independence across the ρ_t's.

2.3 Posterior Computation

With a prior distribution for $(\rho_1, \ldots, \rho_T)$ specified, it remains to determine a model for the response variable which we denote by Y_i with $i = 1, \ldots, m$ for $T = 1$ or Y_{ti} for $T > 1$. The modeling decisions associated with Y_{ti} should be driven by its characteristics. For example, the data scenarios in the Sections 3 and 4 make assuming a conditionally independent Gaussian distribution for $\boldsymbol{Y} = (Y_{11}, \ldots, Y_{Tm})$ appropriate. Once specified, posterior sampling of $\boldsymbol{\rho} \mid \boldsymbol{Y}$ can be achieved by employing the algorithm described in Page et al. (2022). The algorithm requires checking the compatibility between $\rho_0^{\mathfrak{R}}$ and $\rho_1^{\mathfrak{R}}$ for $T = 1$. For $T > 1$ compatibility between $\rho_0^{\mathfrak{R}}$ and $\rho_t^{\mathfrak{R}}$ must be checked for each $t > 1$ under the conditionally independent model and for ρ_{t-1} and ρ_t under the Markovian structure model. Once compatibility is ensured, $\boldsymbol{\rho}$ is updated by sampling the cluster membership allocations c_{ti} and using Algorithm 8 of Neal (2000). In addition, sampling from the full conditional for the $\boldsymbol{\alpha}$ parameters reduces to a simple Beta-Binomial update, while the binary $\boldsymbol{\gamma}$ indicators are easily handled. For more details see Page et al. (2022) and its supplementary material. The computer codes that employ the MCMC algorithm to carry out model fitting in Sections 3 and 4 are available

in the `drpm` R-package that is located at `https://github.com/gpage2990/drpm`.

3   Simulation Studies

In this section we conduct a number of prior and posterior simulation studies to illustrate the behavior of our informed random partition model. Here we present results from a prior simulation study for 10 time points. In section S1 of the supplementary material, we present some results from a prior simulation study with one time point.

3.1   Prior simulation: Multiple time points

We consider $m = 20$ observations and $T = 9$ time points, and use Monte Carlo simulation to generate a sequence of partitions with Markovian dependence $5,000$ times from model in (6). We set ρ_0 to a partition with four clusters each with five units. We use the unit local prior with fixed values $\boldsymbol{\alpha} = (0.25\mathbf{1}_5, 0.5\mathbf{1}_5, 0.75\mathbf{1}_5, 0.95\mathbf{1}_5)$ where $\mathbf{1}_r$ is a vector filled with r ones and set $M = 1$. In Figure 1 we display the 20×20 pairwise co-clustering probability or similarity matrices at each time period. Notice that as time increases the weight of ρ_0 on the pairwise probabilities decreases particularly for those clusters whose α value is small. The cluster that corresponds to $\alpha = 0.95$ has pairwise probabilities that persist (i.e., remain greater than 0.5) even up to the 10th time period.
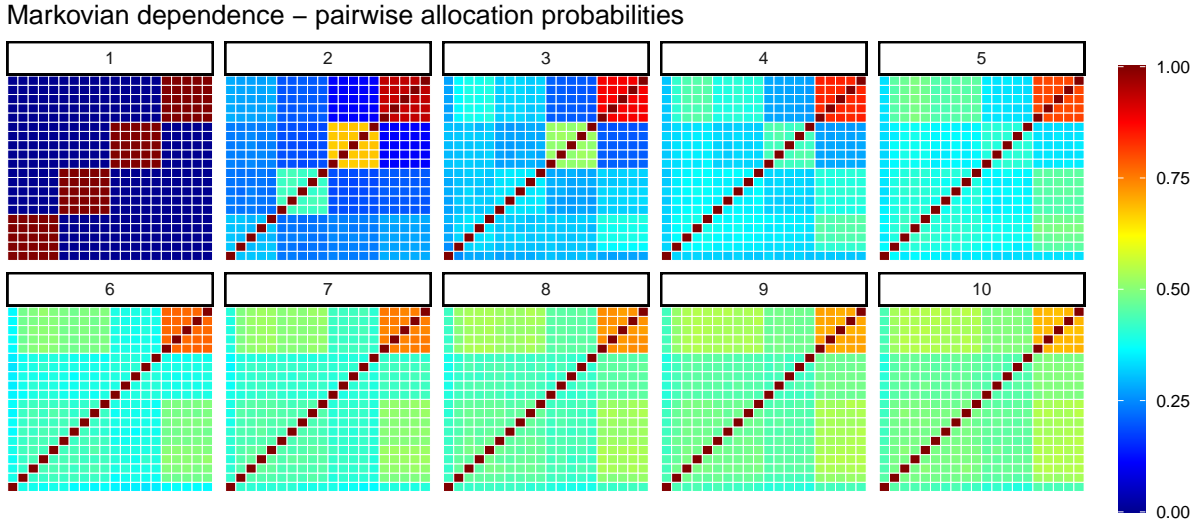
Figure 1: Monte Carlo estimate of pairwise probability matrices. The initial partition ρ_0 is displayed in panel 1 and $\boldsymbol{\alpha} = (0.25\mathbf{1}_5, 0.5\mathbf{1}_5, 0.75\mathbf{1}_5, 0.95\mathbf{1}_5)$

Using the same simulation details as those described previously, we also generated partitions under the conditionally independent case. Then under both informed random partition models, we computed the adjusted Rand index (ARI) proposed in Hubert and Arabie (1985) between ρ_t and ρ_0 denoted by $ARI(\rho_t, \rho_0)$ and the lagged ARI between each time point $ARI(\rho_t, \rho_{t'})$. Figure 2 displays the results. As expected, the time lagged-ARI with ρ_0 decreases under Markovian dependence while remains constant under the conditional independence (right plot of Figure 2). In addition, the pairwise time-lagged ARI under Markovian dependence displays intuitive temporal decay as time between partitions increases, while the conditionally independent remains constant.
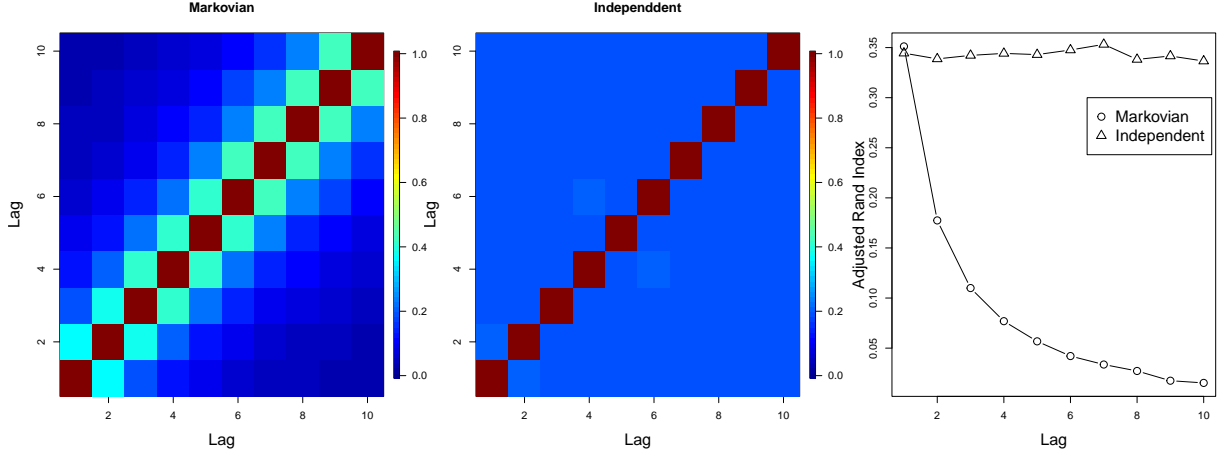
Figure 2: The adjusted Rand index estimates between ρ_t and ρ_0 for each t (right figure) and pairwise between ρ_t and $\rho_{t'}$ for $t \neq t'$ in the markovian case (left figure) and the conditionally independent case (middle figure). ρ_0 is that displayed in panel 1 of Figure 1 with $\boldsymbol{\alpha} = (0.25\mathbf{1}_5, 0.5\mathbf{1}_5, 0.75\mathbf{1}_5, 0.95\mathbf{1}_5)$

3.2 Prior Simulation: comparison with other informative priors

To gain some intuition about the effect of our informed partition model, we consider a simple toy example where we can easily compute and represent the probabilities assigned to each partition. We also compare our proposal with the probability distribution induced by the Centered Partition Process (CPP) proposed in Paganin et al. (2021) and the Location-Scale Partition distribution (LSP) in Smith and Allenby (2020). We briefly summarize these two priors in the following.

The CPP defines a class of priors on the partition space $\mathcal{P}$ that directly penalizes a chosen baseline EPPF $p_0(\cdot)$ to shrink the prior probability mass towards a known partition ρ_0

$$p(\rho \mid \rho_0, \psi) \propto p_0(\rho) \exp\{-\psi d(\rho, \rho_0)\},$$

where $\psi > 0$ is a penalization parameter and $d(\rho, \rho_0)$ a distance metric between partitions. There are many possible choices for the baseline EPPF and of the distances metric; here we

consider the CRP distribution in (5) with concentration parameter M and the Variation of Information (VI), discussed in Meilă (2007), and denote such distribution as $CPP(\rho_0, \psi, M)$. The penalization parameter ψ controls the amount of shrinkage towards ρ_0 with higher values resulting in higher probability mass on partitions close to ρ_0.

The LSP (Smith and Allenby; 2020) is a distribution on $\mathcal{P}$ that is characterized by a location partition (ρ_0) and a scale parameter $\nu > 0$, denoted as $LSP(\rho_0, \nu)$. This last controls the probability mass concentration around ρ_0, with small values favoring partitions closer to ρ_0. The LSP distribution builds on the covariate-dependent PPMs presented in Park and Dunson (2010) and Müller et al. (2011b), treating the location partition ρ_0 as a covariate to inform ρ. The probability mass function induced on $\mathcal{P}$ can be factored into a sequence of conditional probabilities

$$p(\rho \mid \rho_0, \nu) \propto \prod_{i=1}^{m} p(c_i \mid \boldsymbol{c}_{1:(i-1)}, \rho_0, \nu)$$

where $\boldsymbol{c}_{1:(i-1)}$ denotes the vector of cluster membership indicator for unit 1 to $i-1$. We have that for the first indicator $p(c_1 = 1) = 1$ and then

$$p(c_i = k \mid \boldsymbol{c}_{1:(i-1)}, \rho_0, \nu) \propto \begin{cases} \dfrac{\nu + \sum_{l=1}^{i-1} \mathbb{I}\{c_l = k\}\mathbb{I}\{c_{0l} = c_{0i}\}}{\nu K_0^{(i-1)} + \nu + n_k^{(i-1)}} & k = 1, \ldots, K^{i-1} \\ \dfrac{\nu + \mathbb{I}\{c_{0i} = K_0^{i-1}\}}{\nu K_0^{(i-1)} + \nu + 1} & k = K^{i-1} + 1 \end{cases}$$

where $K^{i-1} = \max(c_1, \ldots, c_{i-1})$, $K_0^{i-1} = \max(c_{01}, \ldots, c_{0(i-1)})$, and $n_k^{(i-1)} = \sum_{l=1}^{i-1} \mathbb{I}\{c_l = k\}$ is the number of items in group k among the first $i-1$ items. We refer to Smith and Allenby (2020) for details on the construction and properties of the LSP distribution.

Consider the following toy example: for $m = 5$, there are 52 possible set partitions, and we can easily compute the probability of each partition under different prior distributions. Figure 3 shows the prior probability for each partition induced by the iCRP, the CPP,

and the LSP prior, considering a CRP with $M = 1$. We choose as an initial partition $\rho_0 = \{\{1, 2\}, \{3, 4, 5\}\}$, and use different values for the respective distribution shrinkage parameters. For the iCRP prior we fix the probability α, and consider a spectrum of values between $(0, 1)$. For the CPP, we take the parameter $\psi \in (1, 10)$, while for the LSP prior $\nu \in (0, 3)$.
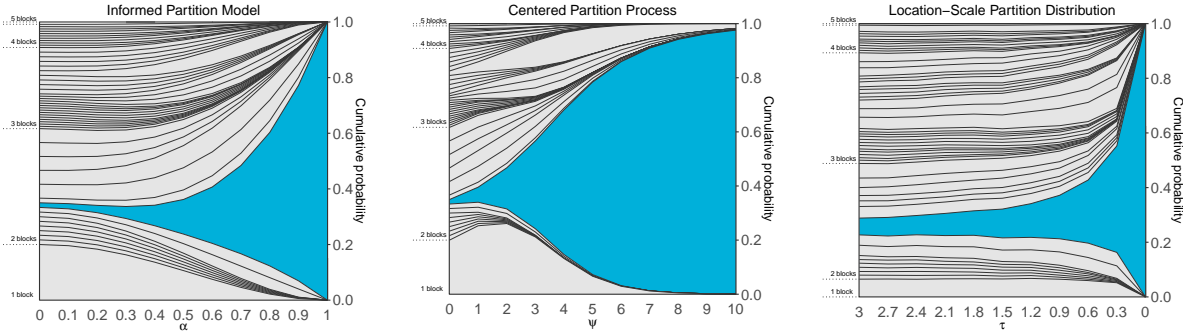

Figure 3: iCRP vs CPP vs LSP. Prior probabilities for each of the 52 partitions when the prior guess is $\rho_0 = \{\{1, 2\}, \{3, 4, 5\}\}$ (highlighted in blue). The cumulative probabilities across different values of the penalization parameters are joined to form the curves, while the probability of a given partition corresponds to the area between the curves. Notice that the x-axis in the third panel is reversed for ease of interpretation.

It is important to remark that the values of the tuning parameters for the three distributions are not directly comparable, as they have different interpretations and scales. Regardless, Figure 3 gives some insights into the different behavior of the three prior distributions and the effect of their shrinkage parameters. The iCRP model and LSP prior convergence to ρ_0, when values of their shrinkage parameter are $\alpha = 1$ and $\nu = 0$ respectively; under the CPP convergence to ρ_0 is formally obtained for $\psi \to \infty$, although in this example for $\psi = 15$ the probability assigned to ρ_0 is roughly 0.99. The iCRP and CPP also include the CRP as a limiting distribution when their shrinkage parameters are equal to zero. Overall, the three priors show different characteristics in how they increase the probability weight of the initial partition, with the iCRP and LSP showing a "concave" shape and the CPP a "convex" one.

The informed partition model can use different α_{ti} values, allowing a more flexible representation of the partition distribution than the one induced by the CPP and LSP priors. We refer to Figure S.10 in the Appendix for an example where we consider different values of these parameters at the unit level.

3.3   Posterior simulation: Proof of Concept With One Time Point

In this simulation study, we explore the impact of our prior construction on recovering the true partition under different scenarios. To this end, we generate data sets of 100 observations, with four clusters each comprised of 25 observations, whose values are randomly generated from a Gaussian distribution. To investigate how cluster separation impacts partition estimates, we set cluster means to $(-h, 0, h, 2h)$, for $h = 1, 2, 3$. Using a standard deviation of 0.5 in all data-generating scenarios, 100 replications are generated per scenario.

We consider the following model where ρ is expressed using cluster labels $c_1, \ldots, c_m$,

$$
\begin{aligned}
Y_i \mid \boldsymbol{\mu}^\star, \boldsymbol{\sigma}^{2\star}, \boldsymbol{c} &\overset{ind}{\sim} N(\mu_{c_i}^\star, \sigma_{c_i}^{2\star}), \ i = 1, \ldots, m \\
(\mu_j^\star, \sigma_j^\star) \mid \theta, \tau^2 &\overset{ind}{\sim} N(\theta, \tau^2) \times UN(0, A_\sigma), \ j = 1, \ldots, k, \\
(\theta, \tau) &\overset{iid}{\sim} N(m_0, s_0^2) \times UN(0, A_\tau), \\
\rho \mid \boldsymbol{\alpha} &\sim iCRP(\rho_0, \boldsymbol{\alpha}, M).
\end{aligned}
\tag{7}
$$

Values of the hyperparameters are chosen as $A_\sigma = \mathrm{sd}(Y)/2$, $m_0 = 0$, $s_0^2 = 100^2$, $A_\tau = 100$, and $M = 1$. We first investigate the effect of our prior construction for fixed values of $\boldsymbol{\alpha}$, while in a second set of simulations, we explore the effect that the prior specification for $\boldsymbol{\alpha}$ has on posterior inference. For the initial partition ρ_0, we consider the following:

- $\rho_0 = \rho_{\text{true}}$: a partition that corresponds to that which generated the data,

- $\rho_0 = \rho_{\text{merge}}$: a partition that contains only two clusters each with 50 units that result in merging clusters with means $(-h, 0)$ and also those with means $(h, 2h)$,

16

- $\rho_0 = \rho_{\text{split}}$: a partition that contains eight clusters by evenly splitting the four original clusters in a random fashion.

An example of each of the ρ_0 partitions we consider is provided in the first row of Figure S.1 of the supplementary material. To each simulated data set, we fit model (7) with $\alpha_{ti} = \alpha$ for all t, i and for each fixed value α ranging over $\{0, 0.25, 0.5, 0.75, 0.9, 0.99\}$.

Model fit was carried out by collecting 1000 MCMC samples after discarding the first 10,000 as burn-in and thinning by 10 (resulting in a total of 20,000 MCMC samples). To measure the accuracy of the partition estimates, we employ the adjusted rand index $ARI(\rho, \rho_0)$. Results are provided in Figure 4.

In Figure 4 the dashed line corresponds to $ARI(\rho_0, \rho_{true})$, the red boxplots correspond to $E(ARI(\rho, \rho_0) \mid \boldsymbol{Y})$ (i.e., $\frac{1}{B} \sum_{b=1}^{B} ARI(\rho^{(b)}, \rho_0)$ where B is the number of posterior samples), and the blue to the $E(ARI(\rho, \rho_{true}) \mid \boldsymbol{Y})$. Notice that as α increases, $E(ARI(\rho, \rho_0) \mid \boldsymbol{Y})$ approaches 1 and $E(ARI(\rho, \rho_{true}) \mid \boldsymbol{Y})$ approaches $ARI(\rho_0, \rho_{true})$. This illustrates the expected behavior that the prior carries more weight in the estimation of ρ as α increases. This, as expected, can negatively affect model fit if ρ_0 is "poorly" specified. To see this, we provide Figure S.2 in the online supplementary material. This figure displays WAIC values (smaller is better) associated with model fit. It turns out that the case in which $\rho_0 = \rho_{\text{merge}}$ results in the largest WAIC value. This is due to the fact that clusters in ρ_{merge} group units with dissimilar measurements unlike the case for ρ_{split} or ρ_{true}.

Using the same synthetic data, we also fit a version of model (7) that treats $\boldsymbol{\alpha}$ as an unknown parameter and employs the global and unit local prior as described in Table 1. This will permit studying how α (or $\boldsymbol{\alpha} = (\alpha_1, \ldots, \alpha_m)$ for the unit local prior) are learned from the data. To this end, we consider for the global prior $\alpha \sim \text{Beta}(1, 1)$, $\alpha \sim \text{Beta}(1, 9)$, or $\alpha \sim \text{Beta}(10, 10)$, and for the unit local prior $\alpha_i \overset{iid}{\sim} \text{Beta}(1, 1)$, $\alpha_i \overset{iid}{\sim} \text{Beta}(1, 9)$, or $\alpha_i \overset{iid}{\sim} \text{Beta}(10, 10)$. Since the prior on $\sigma_j^\star$ also impacts clustering, (clusters are *a posteriori* more homogeneous for smaller values of A_σ), we considered $A_\sigma \in \{0.5, 1, 1.5\}$. Values of
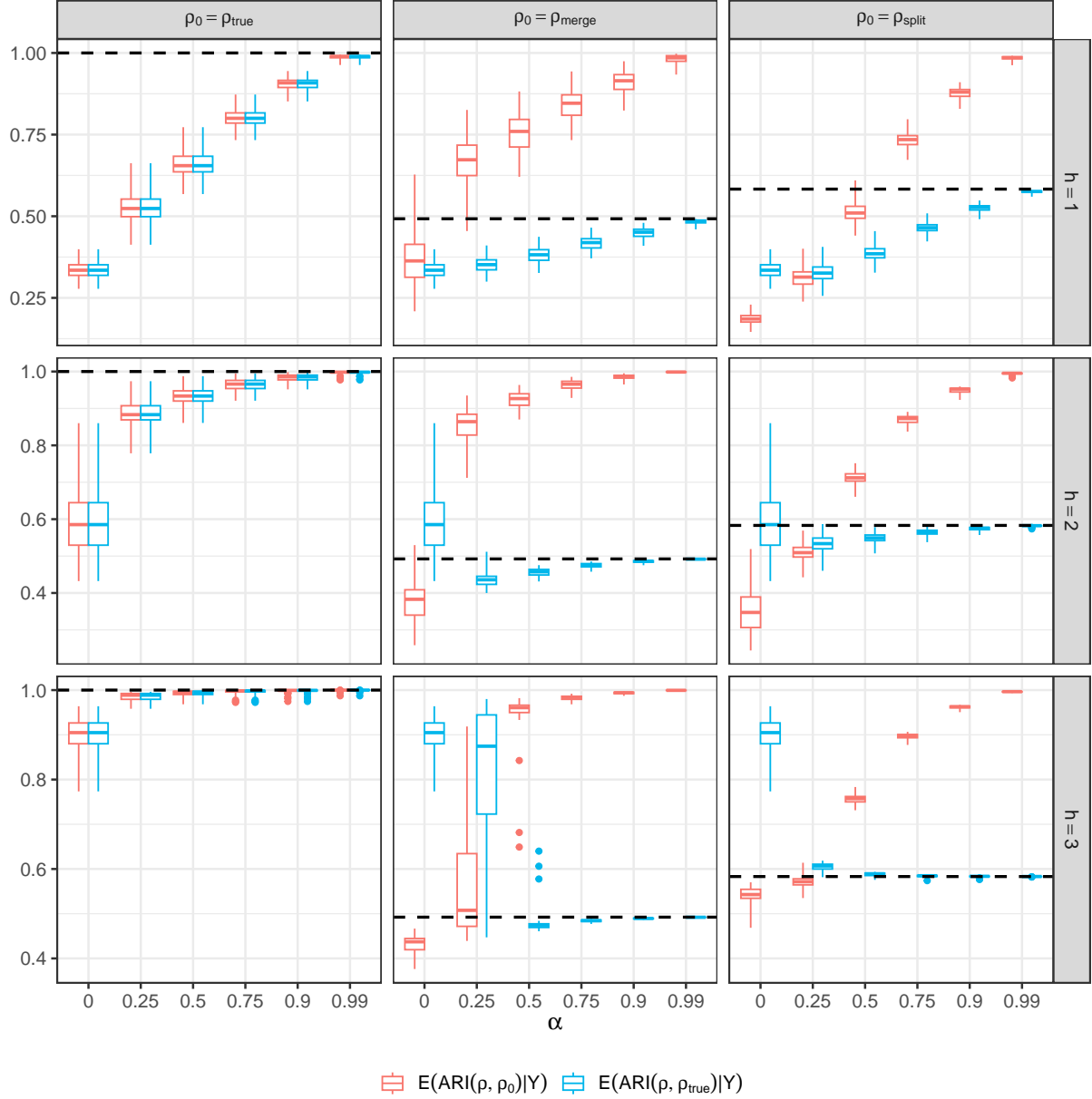
Figure 4: Results for fixed global α. Distribution of $E(ARI(\rho, \rho_0) \mid \boldsymbol{Y})$ (red boxplots) and $E(ARI(\rho, \rho_{true}) \mid \boldsymbol{Y})$ (blue boxplots) across 100 replicated data sets, for each value of $\alpha \in \{0, 0.25, 0.5, 0.75, 0.9, 0.99\}$ are displayed. Each panel shows results for different combinations of the cluster mean separation values used in the data-generating process and the type of initial partition ρ_0. The black dashed line is $ARI(\rho_{\text{true}}, \rho_0)$.

the other hyperparameters are the same as in the previous simulation, where $m_0 = 0$, $s_0^2 = 100^2$, $A_\tau = 100$, and $M = 1$. In addition to exploring different initial partition $\rho_0 \in \{\rho_{\text{true}}, \rho_{\text{merge}}, \rho_{\text{split}}\}$, we also fit the model in (7) without an initial partition (i.e., assume that $\rho \sim CRP(M = 1)$ in (5)). This allows us to understand under which settings the use of prior information aids model estimation. We use the MCMC settings as for the previous simulations. For each replicated data set we recorded the posterior mean of one α parameter when using the global prior, and the average of the posterior means of α_i for $i = 1, \ldots, m$ when using the unit local prior. In addition, we recorded $E(ARI(\rho, \rho_0) \mid \boldsymbol{Y})$ and the log pseudo marginal likelihood (LPML) as defined in Geisser and Eddy (1979).

As expected, the posterior distribution of α is less sensitive to prior specification under the global prior (see Table 1) compared to the unit local prior. Under the unit local prior, the posterior mean of each α_i is pulled towards the prior mean because a single γ_i is informing α_i, for $i = 1, \ldots, m$. However, the trends and comparisons between the different ρ_0 partitions associated for each prior are similar. For this reason here we provide results for the global prior in Figures 5 - 7 and those for unit local prior in the supplementary material (Figures S.3 - S.5).

Figure 5 displays the distribution of $E(\alpha \mid \boldsymbol{Y})$ across 100 replicates for the global prior. Notice that the estimated value of α depends quite heavily on an interaction between the initial partition ρ_0, A_σ, and the informativeness of cluster membership in the data (i.e., the value of h when generating data). Recall that as A_σ decreases, clusters become more homogeneous *a posteriori*. Thus, if the initial partition ρ_0 groups units with response values that are quite different, then the estimated value of α must be small to allow many units to be reallocated. We observe this phenomenon in Figure 5 for $\rho_0 = \rho_{\text{merge}}$ and $A_\sigma = 0.5$. However, since ρ_{split} does not contain clusters with heterogeneous response values, the posterior estimate of α is close to 1 for all values of A_σ, indicating that a relatively small number of units are being moved away from ρ_0. This results in a reduced ARI value (see
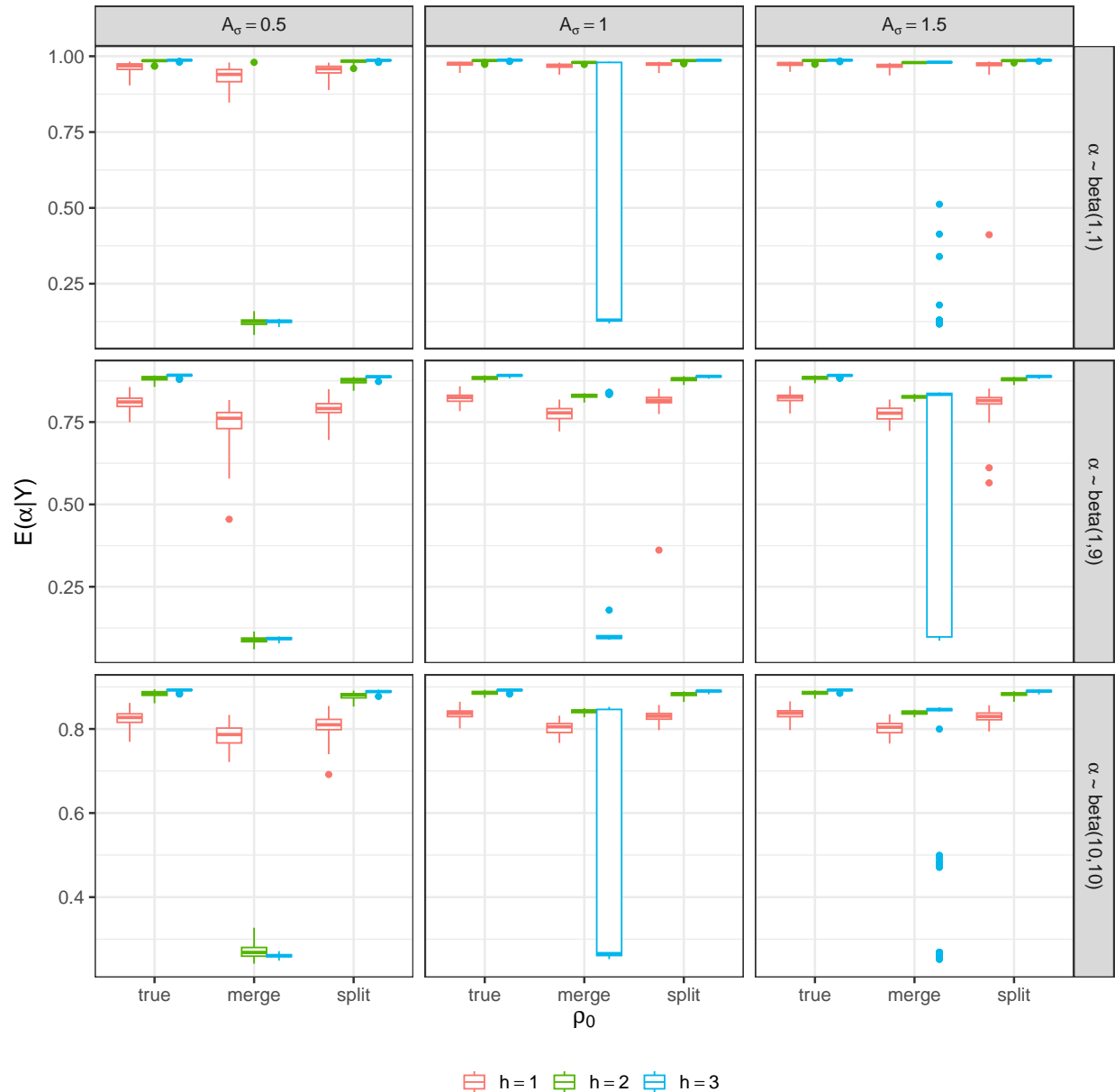
Figure 5: Results for random global α. Distribution of the posterior mean of α for different choices of ρ_0 (x-axis) across 100 replicated data sets using different values for the cluster means separation (boxplot colors). Each panel shows results for different combinations of prior choices for α and A_σ.

Figure 6) as the data are not informative enough to discredit the formation of the extraneous clusters that exist in ρ_0. Evidence of this can be seen in Figure 7 where the LPML values for $\rho_0 = \rho_{\text{split}}$ are quite competitive even though the partition estimate is biased.

With regards to $ARI(\rho, \rho_{true})$, Figure 6 shows that if cluster membership is not well informed by the data (i.e., $h = 1$), then employing any of the ρ_0 we consider provides benefit. However, as cluster membership becomes more informed by data (i.e., $h = 2, 3$), employing an initial partition that allocates units with similar response values into different groups (e.g., ρ_{merge} or ρ_{split}) can adversely affect the partition estimate. This is exacerbated when A_σ is large, which allows for a large likelihood variance favoring heterogeneous clusters. Thus, it seems that the data can "overcome" more readily a misspecified initial partition ρ_0 that has too few clusters (e.g., ρ_{merge}), than one that has too many (e.g., ρ_{split}) if units with similar responses are allocated to different clusters *a priori*. This behavior is somewhat mitigated when using the unit local prior with $\alpha_i \sim \text{Beta}(1, 9)$ which expresses uncertainty with the ρ_0 employed (see Figure S.4 of the supplementary material).

With regards to LPML, Figure 7 shows that including ρ_0 only produces adverse effects when the initial partition groups units that produce quite different response values (e.g., ρ_{merge}). Additionally, this only occurs for higher values of the hyperparameter A_σ, that induce a large likelihood variance. A large likelihood variance permits clusters to be quite heterogeneous and as a result, accommodates a ρ_0 that has heterogeneous clusters. Thus, the use of an initial partition has to be accompanied by careful elicitation of the hyperparameters of the priors for the cluster parameters. Overall, the simulations in this section highlight two main results: i) a reasonable initial partition provides benefit in both, partition estimation and model fit; and ii) the choice of moderately informative hyperparameters for the cluster parameters will have more influence on the posterior estimate of ρ compared to a diffuse prior (which is often the case in Bayesian models).
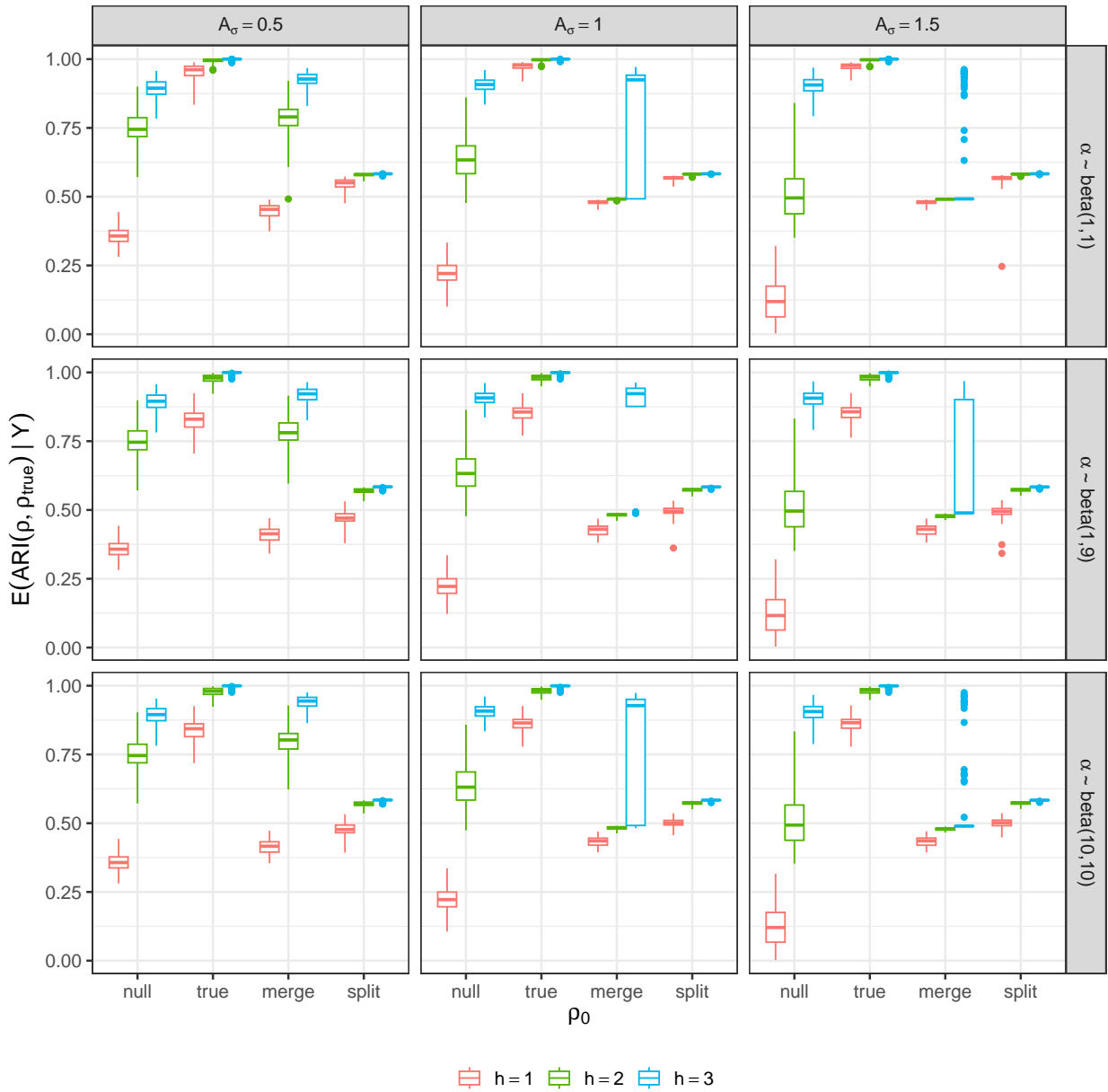
Figure 6: Results for random global α. Distribution of $E(ARI(\rho, \rho_{true}) \mid \boldsymbol{Y})$ for different choices of ρ_0 (x-axis) across 100 replicated data sets using different values for the cluster means separation (boxplot colors). Each panel shows results for different combinations of prior choices for α and A_σ. Here $\rho_0 =$ null corresponds to a model that does not include an initial partition. Notice that when $\rho_0 =$ null results do not change for different values of α, as that parameter is not included in the model.
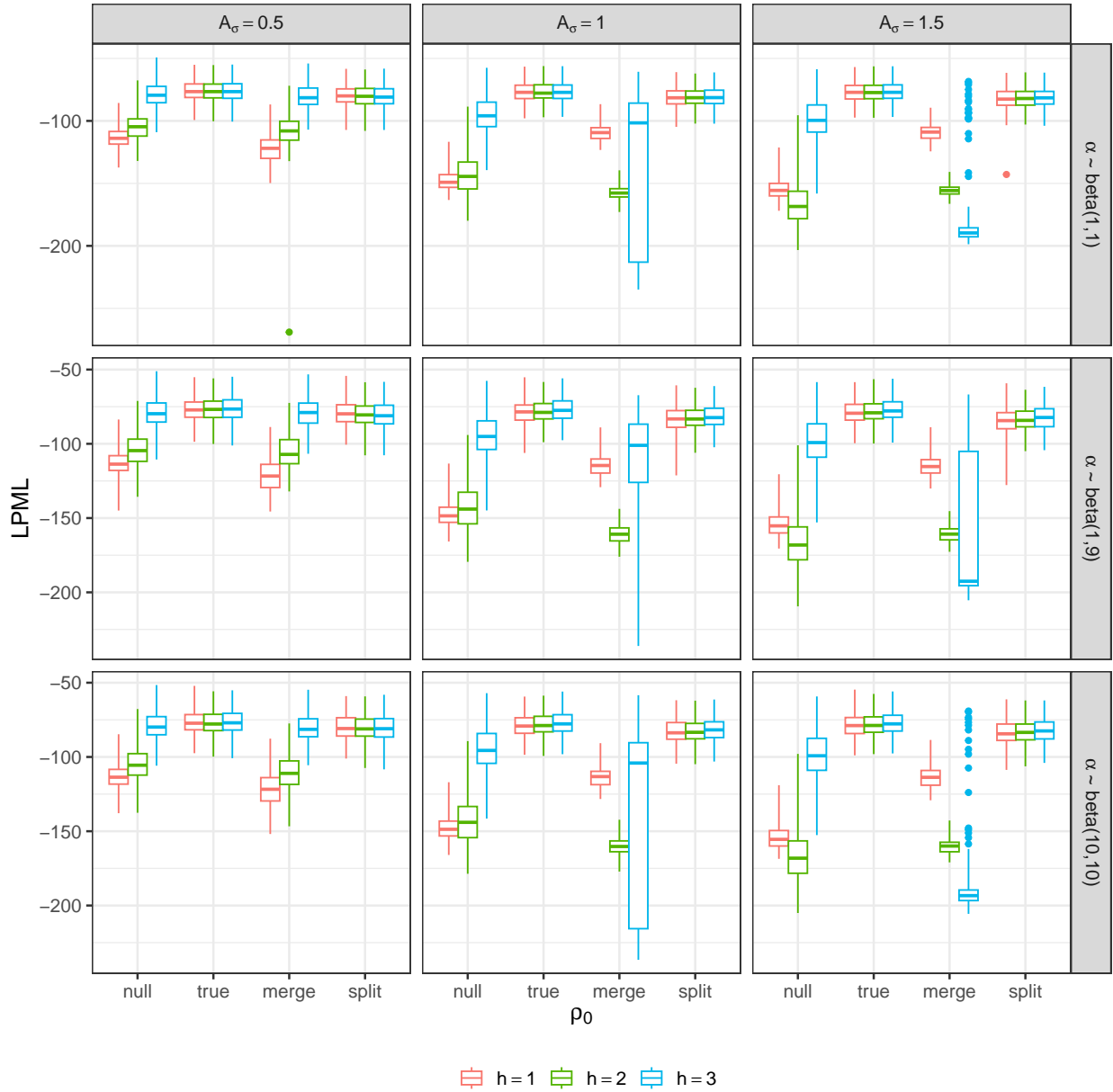
Figure 7: Results for random global α. Distribution of LPML for different choices of ρ_0 (x-axis) across 100 replicated data sets using different values for the cluster means separation (boxplot colors). Larger values of LPML indicate a better fit. Each panel shows results for different combinations of prior choices for α and A_σ. Here $\rho_0 = $ null corresponds to a model that does not include an initial partition. Notice that when $\rho_0 = $ null results do not change for different values of α, as that parameter is not included in the model.

3.4 Posterior simulation: comparison with other informative priors

To compare our construction with those of Paganin et al. (2021) and Smith and Allenby (2020), we consider a small simulation study with data being generated from Gaussian mixtures with different component means and known variance equal to 1. As in Section 3.3, we simulate 100 observations divided into four clusters of equal size, with varying values of the cluster means $(-h, 0, h, 2h)$, for $h = 1, 2, 3$, and use 100 replications for each scenario.

To focus our investigation only on the effect of partition prior, we consider the following simplified version of the model in (7)

$$
\begin{aligned}
Y_i \mid \boldsymbol{\mu}^\star, \boldsymbol{c} &\overset{ind}{\sim} N(\mu_{c_i}^\star, 1), \ i = 1, \ldots, m \\
\mu_j^\star \mid \theta, \tau^2 &\overset{ind}{\sim} N(\theta, \tau^2), \ j = 1, \ldots, k, \\
\rho \mid \rho_0 &\sim p(\rho \mid \rho_0),
\end{aligned}
\tag{8}
$$

where $p(\rho \mid \rho_0)$ indicates an informed prior for the random partition (e.g., iCRP, CPP, or LSP) and hyperparameters are fixed to $\theta = 0$ and $\tau^2 = 10$ across all the choices of partition priors. We considered different choices for the initial partition, with $\rho_0 \in \{\rho_{\text{true}}, \rho_{\text{merge}}, \rho_{\text{split}}\}$. When using our informed partition model, we set $p(\rho \mid \rho_0) = iCRP(\rho_0, \boldsymbol{\alpha}, M)$ in (8), with $M = 1$ and fix $\alpha_{ti} = \alpha$ (all t and i) to the following values $\alpha \in \{0, 0.25, 0.5, 0.75, 0.9, 0.99\}$. When using the CPP, we set $p(\rho \mid \rho_0) = CPP(\rho_0, \psi, M)$ in (8) with $M = 1$ and $\psi \in \{0, 10, 20, 50, 80, 100\}$. For each data set, we ran both models with different values of their tuning parameters for $10,000$ iterations and collected $5,000$ samples after burn-in. Finally, for the LSP prior we set $p(\rho \mid \rho_0) = LSP(\rho_0, \nu)$ and consider different values for the variance parameter, namely $\nu \in \{10, 5, 1, 0.05, 1/(m \log(m)), 0.1/(m \log(m))\}$. Recall that for the LSP prior smaller values represent more informative priors. Since posterior sampling from a model including the LSP prior uses a Metropolis-Hastings algorithm, we consider $50,000$

iterations and discard half of the samples as a burn-in with thinning equal to 5.

Figure 8 shows the distribution of $E(ARI(\rho, \rho_0) \mid \boldsymbol{Y})$ under the three partition priors for the different simulation scenarios. Although values of the tuning parameters are not directly comparable, as the priors become more informative, the $E(ARI(\rho, \rho_0) \mid \boldsymbol{Y})$ values for the iCRP and CPP models converge to $ARI(\rho_{\text{true}}, \rho_0)$, i.e. the posterior distribution for ρ becomes more and more concentrated on the initial partition ρ_0. This also happens for the LSP prior, but not for all the cases. In particular, when $\rho_0 = \rho_{\text{merge}}$ the posterior converges to different partitions for each degree of mean separation h. This also happens when $\rho_0 = \rho_{\text{true}}$ and $h = 1$.

Overall, under the CPP and LSP priors, there is larger variability in the $E(ARI(\rho, \rho_0) \mid \boldsymbol{Y})$ values compared to the iCRP prior and each degree of mean separation h, with $h = 1$ corresponding to the case of largest variability. This can be interpreted as beneficial when using a misspecified initial partition, as in some cases the posterior is concentrated on partitions that are closer to the true one (e.g., $\rho_0 = \rho_{\text{split}}$ and $h \in (2, 3)$ for the CRP, or $\rho_0 = \rho_{\text{merge}}$ and $h = 3$ for the LSP). However, for these two priors, there is higher uncertainty also when the $\rho_0 = \rho_{\text{true}}$, especially when $h = 1$ for the LSP prior which is not desirable. Instead under the iCRP, informative priors lead to small uncertainty in the posterior distribution for the partition, regardless of the initial partition. It is worth mentioning that in this simulation we use a global α parameter for the iCRP, but specifying different degrees of informativeness for each unit can mitigate cases of misspecification of the initial partition.

4   Application

In this section, we consider an environmental science application to further illustrate the utility of our informed partition procedure. As in Section 3, we first consider the case with one time point to focus on the initial partition's impact on partition estimation and model
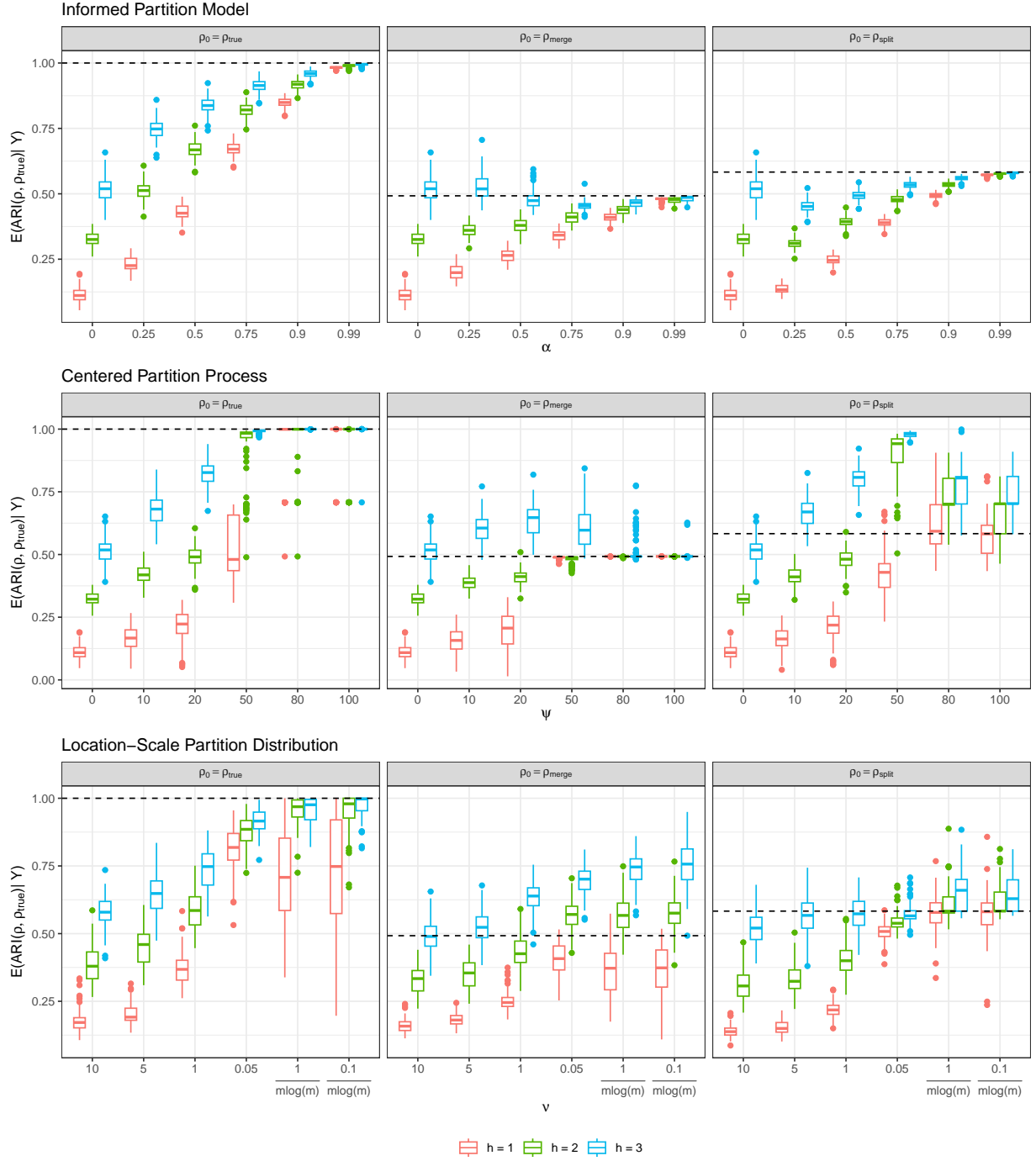
Figure 8: Comparison of posterior results using the iCRP, CPP, and LSP priors for different values of their tuning parameters. Each boxplot represents the distribution of $E(ARI(\rho, \rho_0) \mid \boldsymbol{Y})$ across the 100 generated data sets, with colors distinguishing between data-generating scenarios. The black dashed line is $ARI(\rho_{\text{true}}, \rho_0)$. Notice that the values of the tuning parameters are not directly comparable.

fit and then describe an approach that employs all time points. We now briefly introduce the data.

The rural background PM_{10} dataset is publicly available in the `gstat` package (Gräler et al. 2016) of `R` (R Core Team; 2023). This dataset consists of daily measurements of particulate matter that has a diameter of less than 10μm from 60 atmospheric monitoring stations in rural Germany. Measurements are recorded daily for a number of years, but we focus on average monthly PM_{10} measurements from 2005. In addition to PM_{10} measurements, the longitude and latitude of each monitoring station are recorded.

4.1 PM_{10} Dataset with One Time Point

We first consider data with only one time point by focusing on the average PM_{10} measurements for the month January. To these measurements we fit three models all of which are based on the model employed in Section 3 (see equation (7)). The first, which we call the baseline model, does not supply an initial partition so that a CRP process is used to model ρ. The second and third models include an initial partition (details of which follow) with the former employing a global model for $\boldsymbol{\alpha}$ and the later a unit local model for $\boldsymbol{\alpha}$ (see Table 1).

The initial partition that is employed in global and unit local models is motivated by the spatial nature of atmospheric measurements like PM_{10}. It seems reasonable that the initial partition would contain spatially consistent clusters. To this end, we set ρ_0 to a partition that includes the nine clusters displayed in the top left plot of Figure 9 (Kahle and Wickham 2013). The nine clusters are distinguished in the plot by color and the monitoring stations are enumerated.

Regarding details associated with the model for $\boldsymbol{\alpha}$, for the global model we set $a = 1$ and $b = 9$ so that *a-priori* the probably of a monitoring station moving away form the intial partition is 0.1. For the unit local model of $\boldsymbol{\alpha}$, note from Figure 9 that monitors 36 and
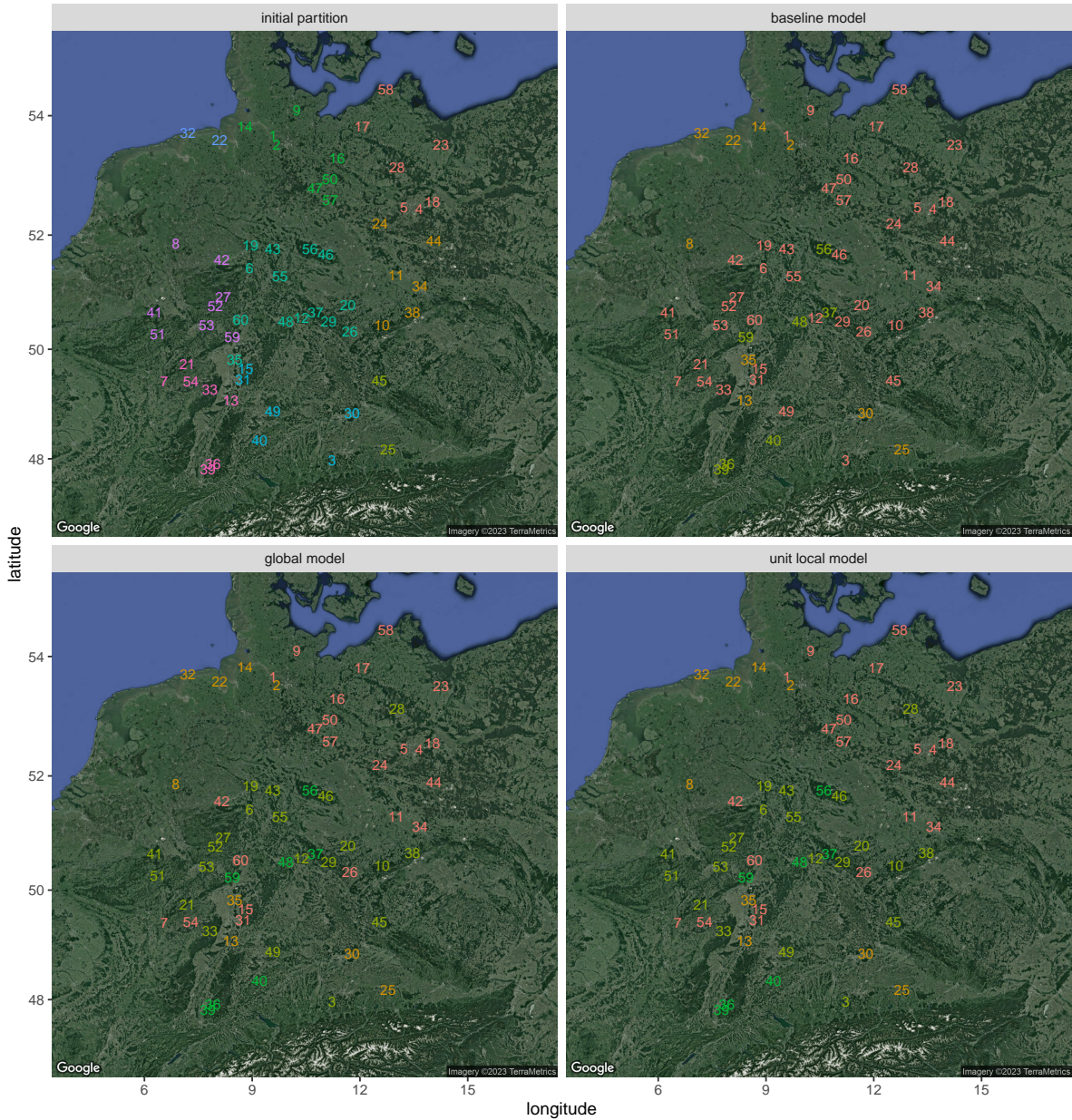
Figure 9: PM$_{10}$ data with number corresponding to station number. The color in each figure corresponds to cluster membership. The top left plot displays the initial partition. The top right displays a partition estimate based on a model with no initial partition (baseline model). The bottom left displays a partition estimate based on a model using the initial partition and a global prior on $\boldsymbol{\alpha}$ (global model). The bottom right displays the partition estimate from a model that includes an initial partition and a local prior for $\boldsymbol{\alpha}$ (unit local model).

39 are both on the same slope of a small mountain located in the south of Germany, while monitors 22 and 32 are in north Germany near the border of the North Sea. As a result, there are geographical reasons for desiring that these stations be in the same cluster. To illustrate how a subset of ρ_0 can be specified with more certainty, for the unit local model we set $a_i = 9$ and $b_i = 1$ for stations 36 and 39 in addition to 22 and 32. For all other stations we set $a_i = 1$ and $b_i = 9$. The former prior specification encourages stations to adhere to ρ_0 while the later encourages stations to move away from ρ_0.

Each of the three models were fit by collecting 1,000 MCMC samples after discarding the first 10,000 as burn-in and thinning by 100. For the hierarchical model specifications we set $A_\sigma = 2.5$, $A_\tau = 100$, $m_0 = 0$, $s_0^2 = 100$, and $M = 1$. To compare the three model fits, we computed the LPML and WAIC values of each model. The results are provided in Table 2. Both LPML and WAIC indicate that models employing ρ_0 fit better than those which do not and that the flexibility of the unit local prior for $\boldsymbol{\alpha}$ results in the best fit.

To obtain a point estimate of the partition for the different models, we minimize the posterior expectation of the variation of information loss (Meilă 2007) using the SALSO method of Dahl, Johnson and Müller (2021) as implemented in the salso R package (Dahl et al. 2022). The partition estimates are provided in Figure 9. Notice that for the baseline model, we estimate one large cluster and two smaller ones, which reflects a clustering behavior typical of the CRP. For the global and unit local $\boldsymbol{\alpha}$ models, the partition estimates are equal and are comprised of four clusters, two of which are medium-sized and two small. Differences in the posterior distributions of the partition between the two models do exist, however. These differences can be seen by way of the co-clustering probabilities, provided in Figure 10. The plots are organized based on partition estimates. That is, the first set of monitoring stations in each of the plots belong to the first cluster, and then those that belong to the second cluster, etc. Notice first that including ρ_0 in the partition model produces partition posterior distributions that seem to be less variable, in the sense that the co-clustering

Table 2: Model fit metrics and posterior co-clustering probabilities between station 22 and 32 and between 36 and 39 along with LPML (larger is better) and WAIC (lower is better) for the three models fit to data from the month of January in the PM_{10} data.

model	LPML	WAIC	$Pr(c_{22} = c_{32} \mid \boldsymbol{Y})$	$Pr(c_{36} = c_{39} \mid \boldsymbol{Y})$
baseline (no ρ_0)	-192.65	315.37	0.71	0.69
global for $\boldsymbol{\alpha}$	-184.84	291.00	0.58	0.71
unit local for $\boldsymbol{\alpha}$	-172.31	281.15	0.77	0.98
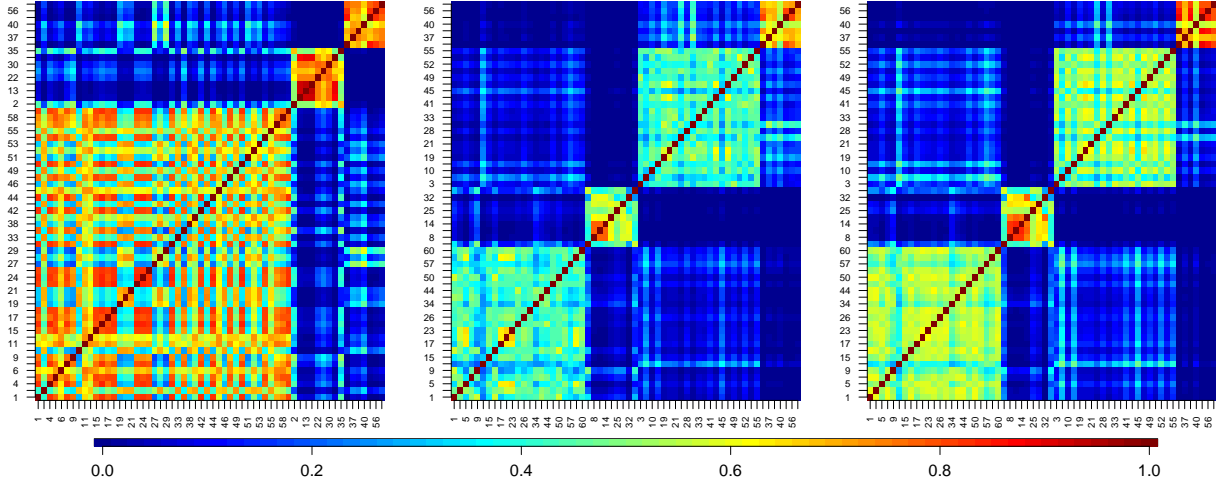
Figure 10: Posterior co-clustering probabilities for baseline (left), global (middle) and unit local (right) models.

probabilities of monitoring stations within a cluster are all above 0.5 which is not the case for the baseline model. Co-clustering probabilities from the global and unit local models are similar, but it seems that the unit local model produces co-clustering probabilities among grouped stations that are closer to one compared to those from the global model. Table 2 lists the co-clustering probabilities for stations 22 and 32 in addition to stations 36 and 39. Notice that both co-cluster probabilities are largest for the unit local model. The global model has the smallest co-clustering probability for stations 22 and 32. These results highlight how users can have varying levels of certainty associated with subsets of the initial partition.

4.2 PM$_{10}$ Dataset with Multiple Time Points

Next we consider all $T = 12$ months of average PM$_{10}$ measurements from the year 2005. To incorporate the idea of temporal dependence in the partition model, we consider the following hierarchical model that is similar to that in Page et al. (2022)

$$
\begin{aligned}
Y_{it} \mid \boldsymbol{\mu}_t^\star, \boldsymbol{\sigma}_t^{2\star}, \boldsymbol{c}_t &\stackrel{ind}{\sim} N(\mu_{c_{it}t}^\star, \sigma_{c_{it}t}^{2\star}), \ i = 1, \ldots, m \text{ and } t = 1, \ldots, T, \\
(\mu_{jt}^\star, \sigma_{jt}^\star) \mid \theta_t, \tau_t^2 &\stackrel{ind}{\sim} N(\theta_t, \tau_t^2) \times UN(0, A_\sigma), \ j = 1, \ldots, k_t, \\
(\theta_t, \tau_t) &\stackrel{iid}{\sim} N(\phi_0, \lambda^2) \times UN(0, A_\tau), \ t = 1, \ldots, T, \\
(\phi_0, \lambda) &\sim N(m_0, s_0^2) \times UN(0, A_\lambda), \\
\rho_t \mid \rho_{t-1} &\sim iCRP(\rho_{t-1}, \boldsymbol{\alpha}, M), \ t = 1, \ldots, T, \\
\alpha_{ti} &\sim Beta(a_{ti}, b_{ti}).
\end{aligned}
\tag{9}
$$

Here $UN(\cdot)$ denotes a uniform distribution and for hyper-parameters we used $A_\sigma = 2.5$, $A_\tau = 100$, $A_\lambda = 5$, $m_0 = 0$, $s_0^2 = 100$, and $M = 1$. Values of a_{ti} and b_{ti} are detailed shortly.

To these data, we fit the model in (9) by considering five different prior specifications for $\boldsymbol{\rho}$. As before, the baseline model corresponds to that which does not supply ρ_0, while the other four models use the same initial partition ρ_0 as in Section 4.1 and the four models for $\boldsymbol{\alpha}$ detailed in Table 1. For the global model $a = 1$ and $b = 9$ and for the time local model $a_t = 1$ and $b_t = 9$ for all t. For the unit local model $a_i = 1$ and $b_i = 9$ for all i except for $i \in \{22, 32, 36, 39\}$ for which $a_i = 9$ and $b_i = 1$ (as was done in the Section 4.1). Finally for the time $\times$ unit model $a_{it} = 1$ and $b_{it} = 9$ for all t and i except that for $i \in 22, 32, 36, 39$ we set $a_{it} = 9$ and $b_{it} = 1$ for all t. Using these prior distributions for $\boldsymbol{\rho}$ we fit model (9) by collecting 2000 MCMC samples after discarding the first 50,000 as burnin and thinning by 50 (a total of 150,000 MCMC iterates were sampled).

The LPML and WAIC for each model are provided in Table 3. The unit$\times$time local and baseline priors appear to result in the worst data fit. There is a clear indication that

borrowing strength across units or time does improve model fit as the unit local and time local priors fit the best. Thus, including ρ_0 provides value in terms of model fit, but the added value diminishes as the model becomes too flexible. In fact, the unit×time local prior is so flexible that the posterior distribution of each α_{ti} depends heavily on the values selected for a_{ti} and b_{ti}.

Figure 11 illustrates how the different models influence the co-clustering probabilities between stations 22 and 32 and stations 36 and 39 across time. The left margin labels each row's co-clustering probability (either $Pr(c_{22} = c_{32} \mid \mathbf{Y})$ or $Pr(c_{36} = c_{39} \mid \mathbf{Y})$) and the right margin indicates to which model each row corresponds. Notice that $Pr(c_{36} = c_{39} \mid \mathbf{Y})$ is fairly large across time for all models. However, for models that incorporate ρ_0, $Pr(c_{22} = c_{32} \mid \mathbf{Y})$ seems to decrease over time. This seemed counterintuitive at first glance since the prior on $\boldsymbol{\alpha}$ for these models together with ρ_0 encourages stations 22 and 32 to co-cluster. However, upon further inspection of the data, it appears that station 32's PM$_{10}$ measurements are fairly different from those from the other stations (and in particular station 22). Figure 12 illustrates this along with partition estimates for each model at each time point (as before partition estimation is carried out using the `salso` R-package by Dahl, Johnson and Müller 2021). The first thing to notice from this figure is that the baseline model results in stations 22 and 32 being clustered together at each time point even though there are instances when their measurements are quite different. This is due to a large estimated α value (95% interval of (0.83,0.91)) which results in fairly static partitions over time that are based on a CRP type partition at time period 1. Conversely, introducing ρ_0 in the global model results in stations 22 and 32 only being clustered at time periods 1 and 4. The reason for this is that α is estimated to be smaller compared to the baseline model (95% interval of (0.75,0.84)). This is due to the fact that ρ_0 and the time 1's PM$_{10}$ measurements only marginally agree necessitating a larger percentage of units to be reallocated at time 1 which in turn requires a smaller value of α. Thus, it appears that when estimating partitions over time is desired, our

32

Table 3: LPML (larger is better) and WAIC (smaller is better) for four models fit to the data.

model	LPML	WAIC
baseline (no ρ_0)	-1952.85	3359.26
global for $\boldsymbol{\alpha}$	-1957.01	3043.59
unit local for $\boldsymbol{\alpha}$	-1650.47	3015.55
time local for $\boldsymbol{\alpha}$	-1889.57	2974.56
unit×time local for $\boldsymbol{\alpha}$	-3678.83	3416.42

method provides sufficient flexibility to produce partition estimates with more homogeneous clusters (compared to models that do not include ρ_0).

Lastly, Figure 13 displays the time-lagged ARI value for each model. It appears that the baseline model produces partition estimates whose temporal dependence decays more slowly compared to the models that include ρ_0 (see the top left plot of Figure 13). This is because the baseline model had the highest estimate value for α resulting in less reallocation of stations. The time × local model displays essentially no temporal dependence among the partitions. This model introduces too much flexibility as there is an α parameter for each station and time period making the prior quite influential and as a result, α_{it} values are all near 0.5. The other three models that include ρ_0 demonstrate varying degrees of temporal dependence decay between partitions estimates. The decay was accelerated when α was not fixed across time. The time-lagged ARI results are different between the baseline and global models for the same reasons outlined in the previous paragraph.
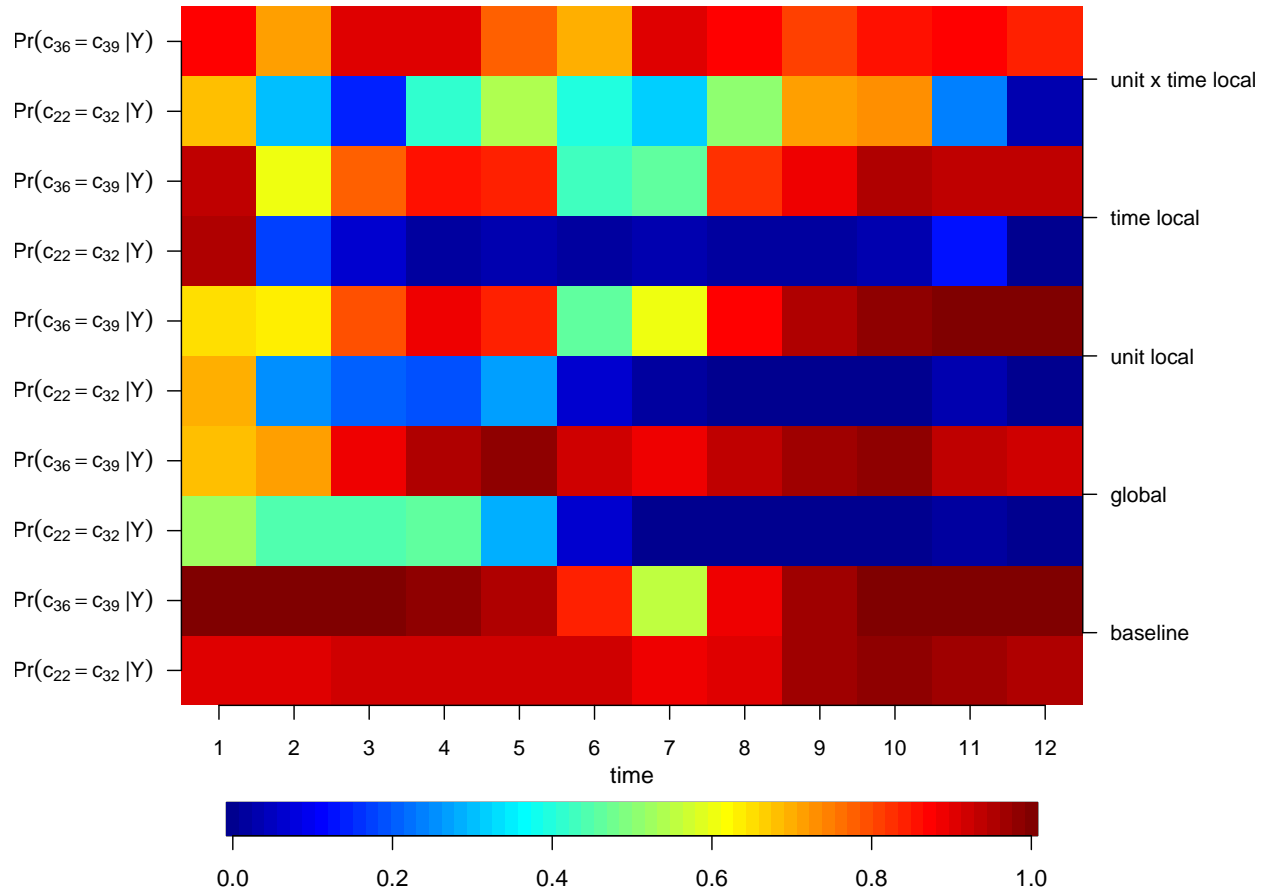
Figure 11: Posterior co-clustering probabilities across time between stations 22 and 32 and between stations 36 and 39 for each of the five models fit to the PM$_{10}$ data.
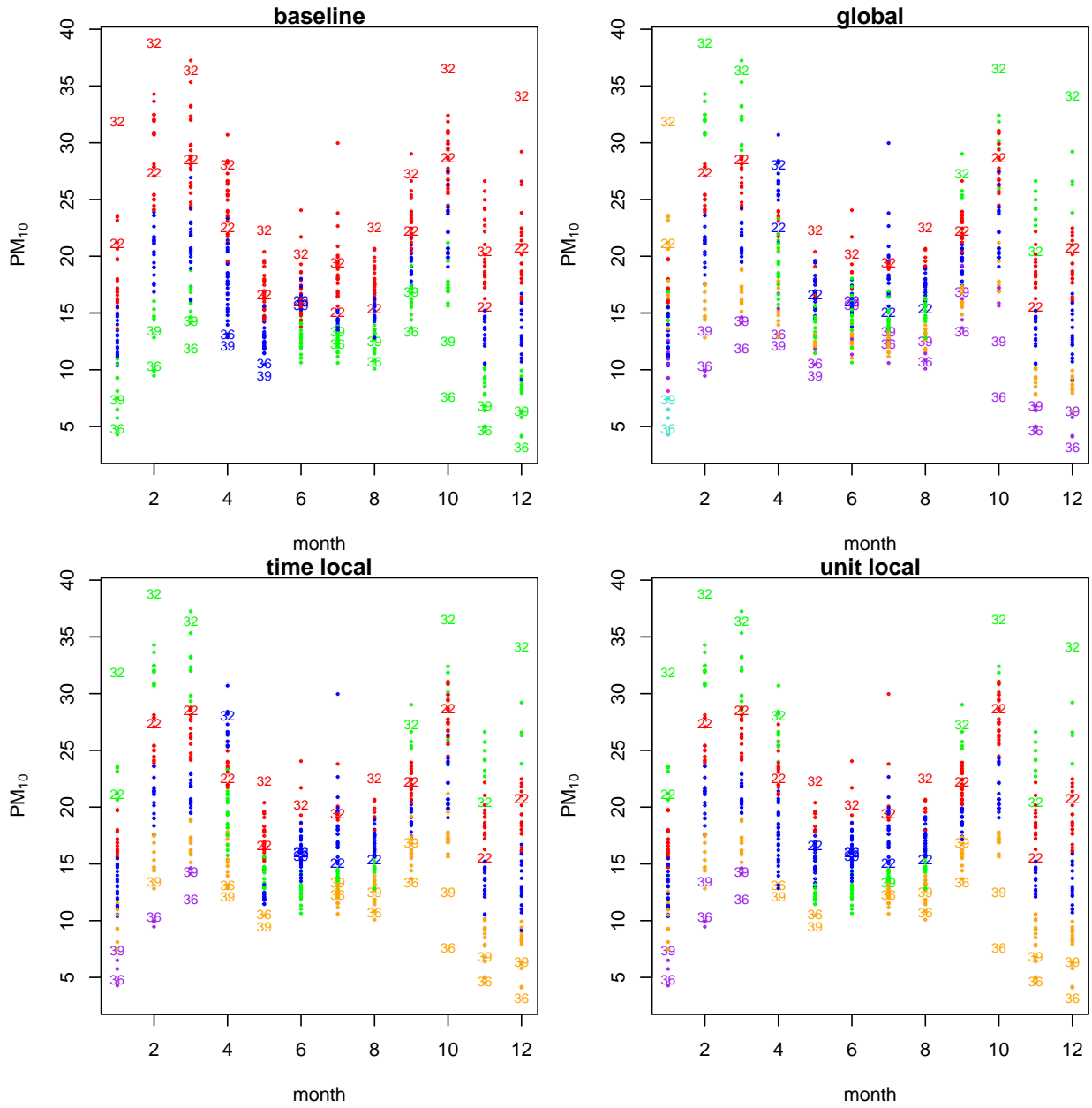
Figure 12: PM_{10} measurements from each of the 60 stations across the 12 months. Stations 22, 32, 39, and 36 are highlighted using their respective numbers. The color indicates group membership. The top left plot corresponds to the baseline model fit, the top right to that of the global α prior, the bottom left to the time local, and the bottom right to the unit local prior for α.
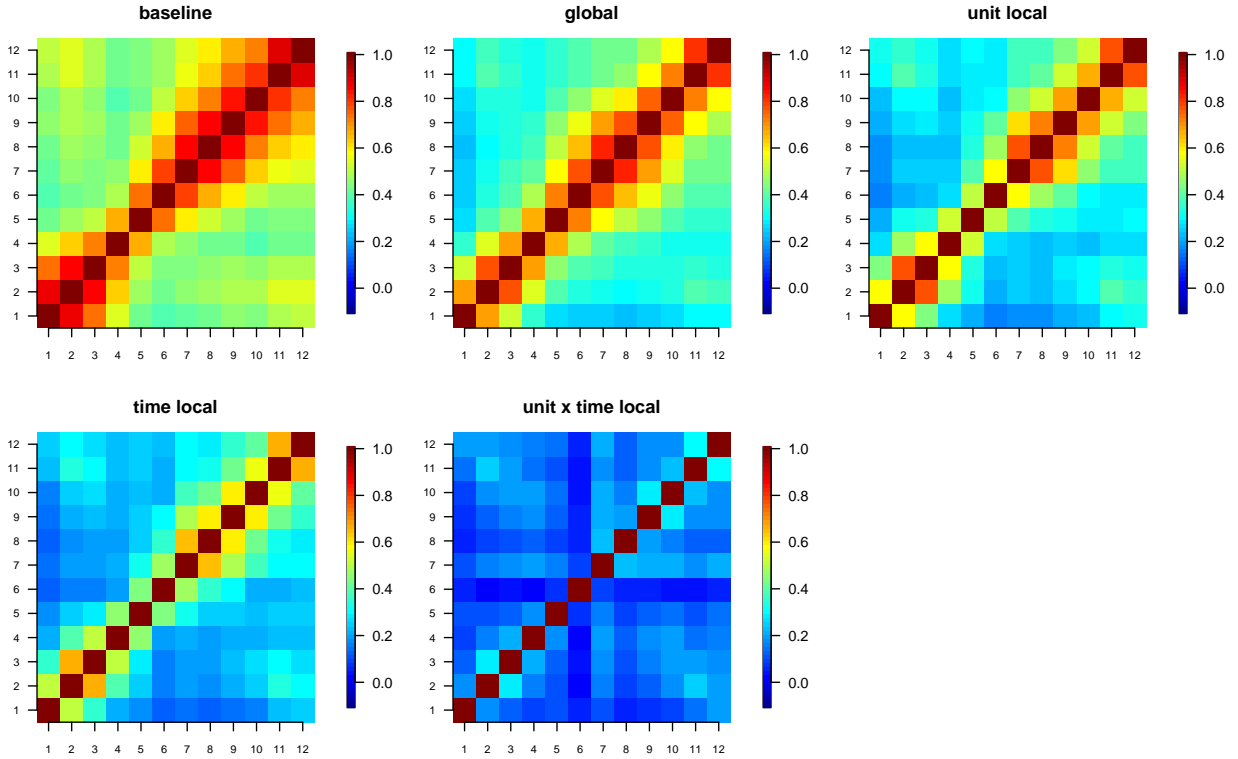
Figure 13: Posterior means for the time-lagged adjusted rand index associated with each of the five models fit to the PM_{10} data.

5 Summary and Discussion

In this work we propose probability model for a sequence of random partitions of $[m]$, with the ability to incorporate prior information in the form of a given partition ρ_0 that contains subsets judged to be a priori more likely to appear. The model has the ability also of up- or down-weighting different subsets in ρ_0, thus effectively reflecting various degrees of certainty on these subsets. Through extensive simulation studies, the model was shown to perform well compared to alternatives that also incorporate such prior information. Application to a dataset on PM_{10} measurements in Germany shows the benefits of our proposed model.

For the purpose of illustrating the approach (through simulations and data analysis) we have adopted simple Gaussian likelihood models. Nevertheless, the methods can be easily

extended to cover other specifications, such as including the case of non-Gaussian responses and/or serial correlation over time points. Similarly, the EPPF in (4) may be easily extended to include covariate dependence, e.g, as in a PPMx-like model.

A possible avenue of further research would be to introduce some structure in the prior distribution of $\boldsymbol{\gamma}$. That is, consider the binary γ_{ti} parameters, postulate an autologistic model such as CAR or similar model. Here, the correlation structure of the CAR-like model would be such that units i and j are neighbors if and only if they belong to the same cluster.

Acknowledgments

References

Argiento, R., Filippi-Mazzola, E. and Paci, L. (2022). Model-based clustering of categorical data based on the hamming distance. *arXiv:2212.04746v1.*

Dahl, D. B., Day, R. and Tsai, J. W. (2017). Random partition distribution indexed by pairwise information, *Journal of the American Statistical Association* **112**(518): 721–732.

Dahl, D. B., Johnson, D. J. and Müller, P. (2021). *salso: Search Algorithms and Loss Functions for Bayesian Clustering.* R package version 0.3.0.
URL: *https://CRAN.R-project.org/package=salso*

Dahl, D. B., Johnson, D. J. and Müller, P. (2022). Search algorithms and loss functions for bayesian clustering, *Journal of Computational and Graphical Statistics* **31**(4): 1189–1201.

Dahl, D. B., Warr, R. and Jensen, T. (2021). Shrinking a partition distribution towards a baseline partition, with applications to dependent partitions. *Presentation in the BNP Section of ISBA webinar series.*
URL: *https://www.youtube.com/watch?v=FKxc6l49Vv8*

Ferguson, T. S. (1973). A Bayesian analysis of some nonparametric problems, *The Annals of Statistics* **1**: 209–230.

Franzolini, B., Iorio, M. D. and Eriksson, J. (2023). Conditional partial exchangeability: a probabilistic framework for multi-view clustering. *arXiv:2307.01152v1.*

Geisser, S. and Eddy, W. F. (1979). A predictive approach to model selection, *Journal of the American Statistical Association* **74**(365): 153–160.

Gräler, B., Pebesma, E. and Heuvelink, G. (2016). Spatio-temporal interpolation using gstat, *The R Journal* **8**: 204–218.
URL: *https://journal.r-project.org/archive/2016-1/na-pebesma-heuvelink.pdf*

Grazian, C. (2023). A review on bayesian model-based clustering. *arXiv:2303.17182v2*.

Hartigan, J. A. (1990). Partition models, *Communications in Statistics. Theory and Methods* **19**: 2745–2756.

Hubert, L. and Arabie, P. (1985). Comparing partitions, *Journal of Classification* **2**: 193–218.

Kahle, D. and Wickham, H. (2013). ggmap: Spatial visualization with ggplot2, *The R Journal* **5**(1): 144–161.
URL: *https://journal.r-project.org/archive/2013-1/kahle-wickham.pdf*

Lijoi, A., Prünster, I. and Rigon, T. (2023). Finite-dimensional discrete random structures and bayesian clustering, *Journal of the American Statistical Association* **0**(0): 1–13. In press.
URL: *https://doi.org/10.1080/01621459.2022.2149406*

Meilă, M. (2007). Comparing clusterings - an information based distance, *Journal of Multivariate Analysis* **98**(5): 873 – 895.

Müller, P., Quintana, F. A., Jara, A. and Hanson, T. (2015). *Bayesian Nonparametric Data Analysis*, Springer.

Müller, P., Quintana, F. and Rosner, G. L. (2011a). A product partition model with regression on covariates, *Journal of Computational and Graphical Statistics* **20**(1): 260–278. Supplementary material available online.

Müller, P., Quintana, F. and Rosner, G. L. (2011b). A product partition model with regression on covariates, *Journal of Computational and Graphical Statistics* **20**(1): 260–278.

Neal, R. M. (2000). Markov chain sampling methods for dirichlet process mixture models, *Journal of Computational and Graphical Statistics* **9**: 249–265.

Ni, Y., Müller, P., Diesendruck, M., Williamson, S., Zhu, Y. and Ji, Y. (2020). Scalable bayesian nonparametric clustering and classification, *Journal of Computational and Graphical Statistics* **29**(1): 53–65.
URL: *https://doi.org/10.1080/10618600.2019.1624366*

Paganin, S., Herring, A. H., Olshan, A. F. and Dunson, D. B. (2021). Centered Partition Processes: Informative Priors for Clustering (with Discussion), *Bayesian Analysis* **16**(1): 301 – 670.
URL: *https://doi.org/10.1214/20-BA1197*

Page, G. L., Quintana, F. A. and Dahl, D. B. (2022). Dependent modeling of temporal sequences of random partitions, *Journal of Computational and Graphical Statistics* **31**(2): 614–627.

Park, J.-H. and Dunson, D. B. (2010). Bayesian generalized product partition model, *Statist. Sinica* **20**(3): 1203–1226.

Pitman, J. (1995). Exchangeable and partially exchangeable random partitions, *Probability Theory and Related Fields* **102**(2): 145–158.

Pitman, J. (1996). Some developments of the Blackwell-MacQueen urn scheme, *Statistics, probability and game theory*, Vol. 30 of *IMS Lecture Notes Monogr. Ser.*, Inst. Math. Statist., Hayward, CA, pp. 245–267.

R Core Team (2023). *R: A Language and Environment for Statistical Computing*, R Foundation for Statistical Computing, Vienna, Austria.
URL: *https://www.R-project.org*

Regazzini, E., Lijoi, A. and Prünster, I. (2003). Distributional results for means of normalized random measures with independent increments, *The Annals of Statistics* **31**(2): 560–585. Dedicated to the memory of Herbert E. Robbins.

Smith, A. N. and Allenby, G. M. (2020). Demand models with random partitions, *Journal of the American Statistical Association* **115**(529): 47–65.

Wade, S. (2023). Bayesian cluster analysis, *Philosophical Transactions of the Royal Society A: Mathematical, Physical and Engineering Sciences* **381**(2247): 20220149.

S.1 Additional Simulation Study Results

The top row of Figure S.1 correspond to the initial partitions that were considered in the simulation study detailed in Section 3.3. We also considered initial partitions that are displayed in the second and third rows of Figure S.1, the results of which are described shortly. First however, we describe in a bit more detail WAIC results and then those associated with the unit local model for $\boldsymbol{\alpha}$. Figure S.2 display the WAIC values associated with the different partitions as a function of ρ_0, h, and α (see Section 3.3 of the main document for more details). Note that model fits are quite similar overall, with the initial partition ρ_{merge} generally speaking resulting in the best fits, while initial partition ρ_{split} performing similarity to not including an initial partition at all.
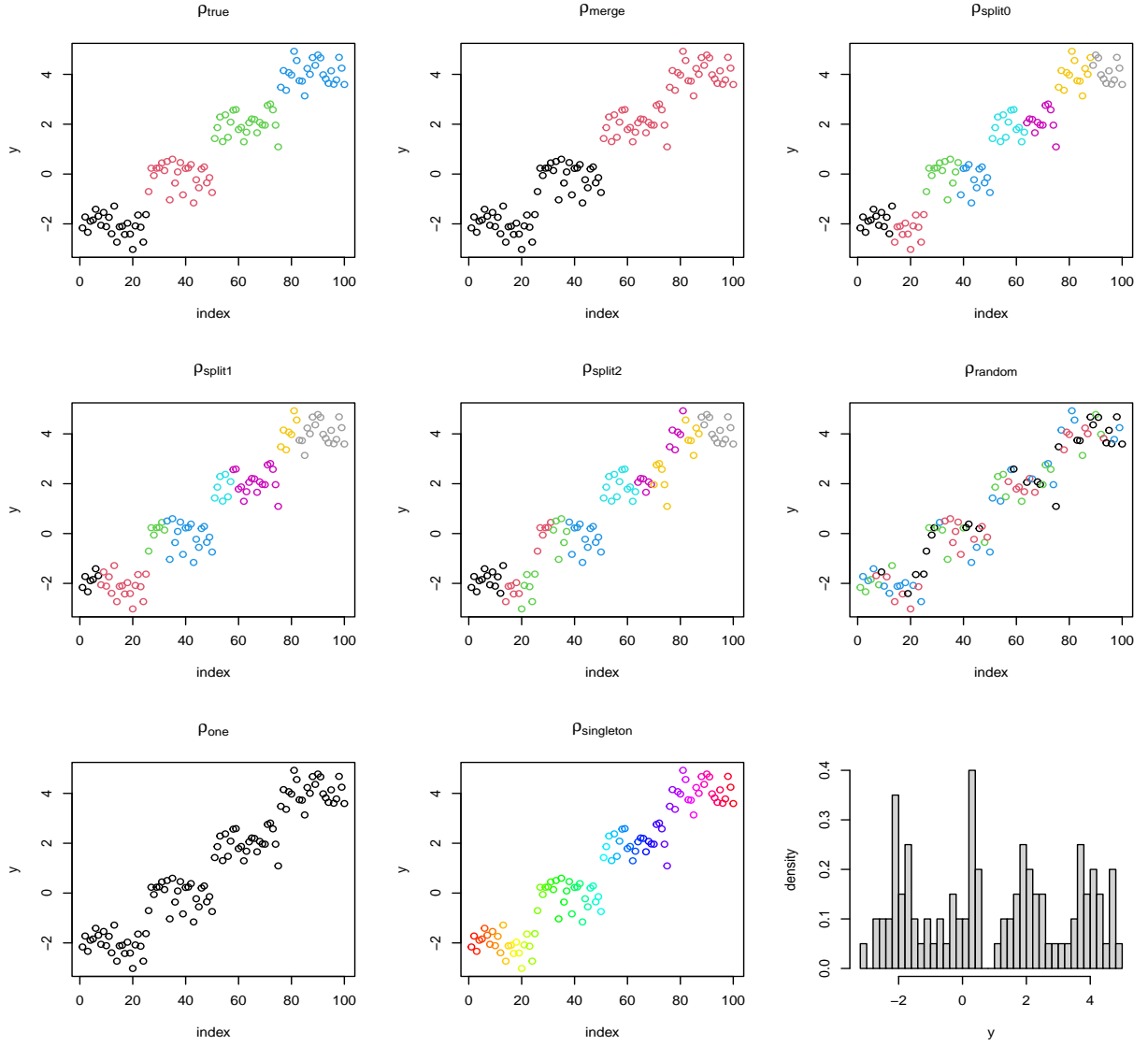
Figure S.1: synthetic data (bottom-right panel) and the eight initial partitions employed.

Figure S.3 displays the average of the posterior means for $\alpha_i, i = 1, \ldots, m$ under the unit local model. As expected there are differences between the two. This is a consequence of the number of γ_i's that are used to estimate them, as required by the model. Notice that for the global α model the posterior means of α are more concentrated towards 0 or 1 and are less influenced by the prior distributions. This is because all m γ parameters are used when estimating α. With regards to the partitions, it seems that when formulating an initial partition one should err on the side of being parsimonious. It appears that if the initial partition contains more clusters than the true partition, then one must apply quite a bit of prior weight away from the initial partition or it remains heavily weighted. This is less so for the local α model.

41
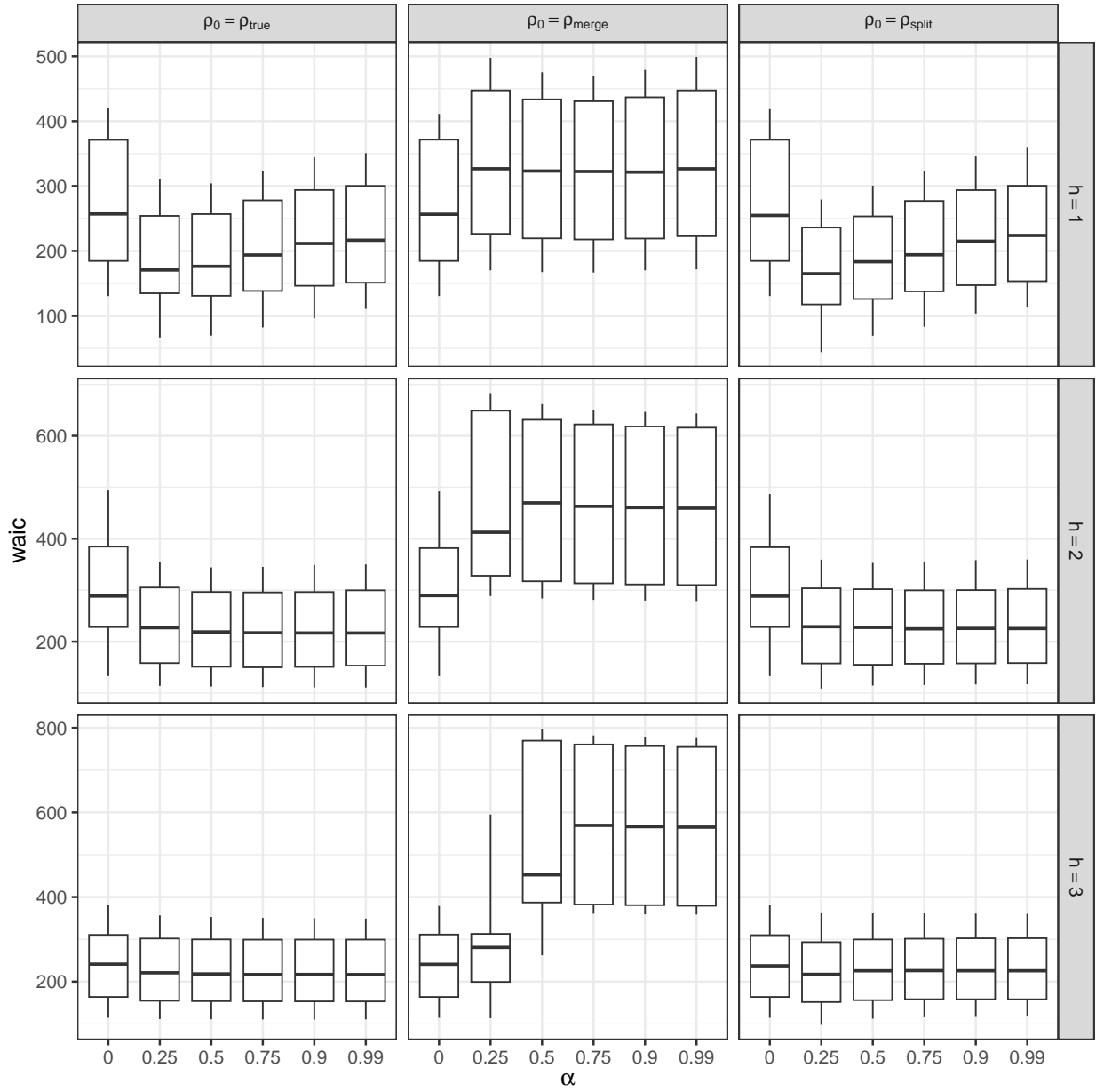
Figure S.2: Results for fixed global α. Distribution of WAIC across 100 replicated data sets, for each value of $\alpha \in \{0, 0.25, 0.5, 0.75, 0.9, 0.99\}$ are displayed. Each panel shows results for different combinations of the cluster mean separation values used in the data-generating process and the type of initial partition ρ_0.
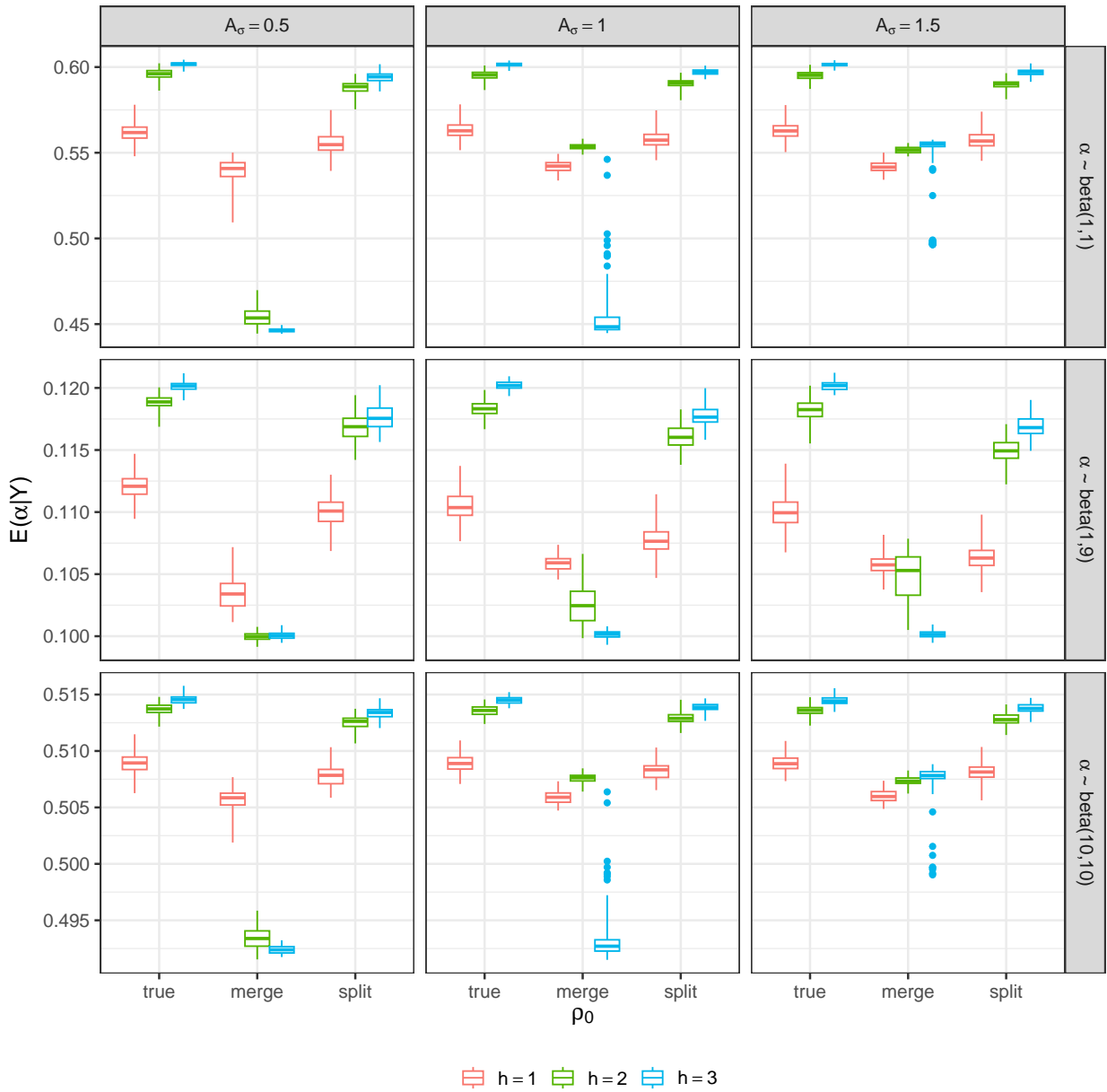
Figure S.3: Results for unit local random α. Distribution of the posterior mean of α for different choices of ρ_0 (x-axis) across 100 replicated data sets using different values for the cluster means separation (boxplot colors). Each panel shows results for different combinations of prior choices for α and A_σ.
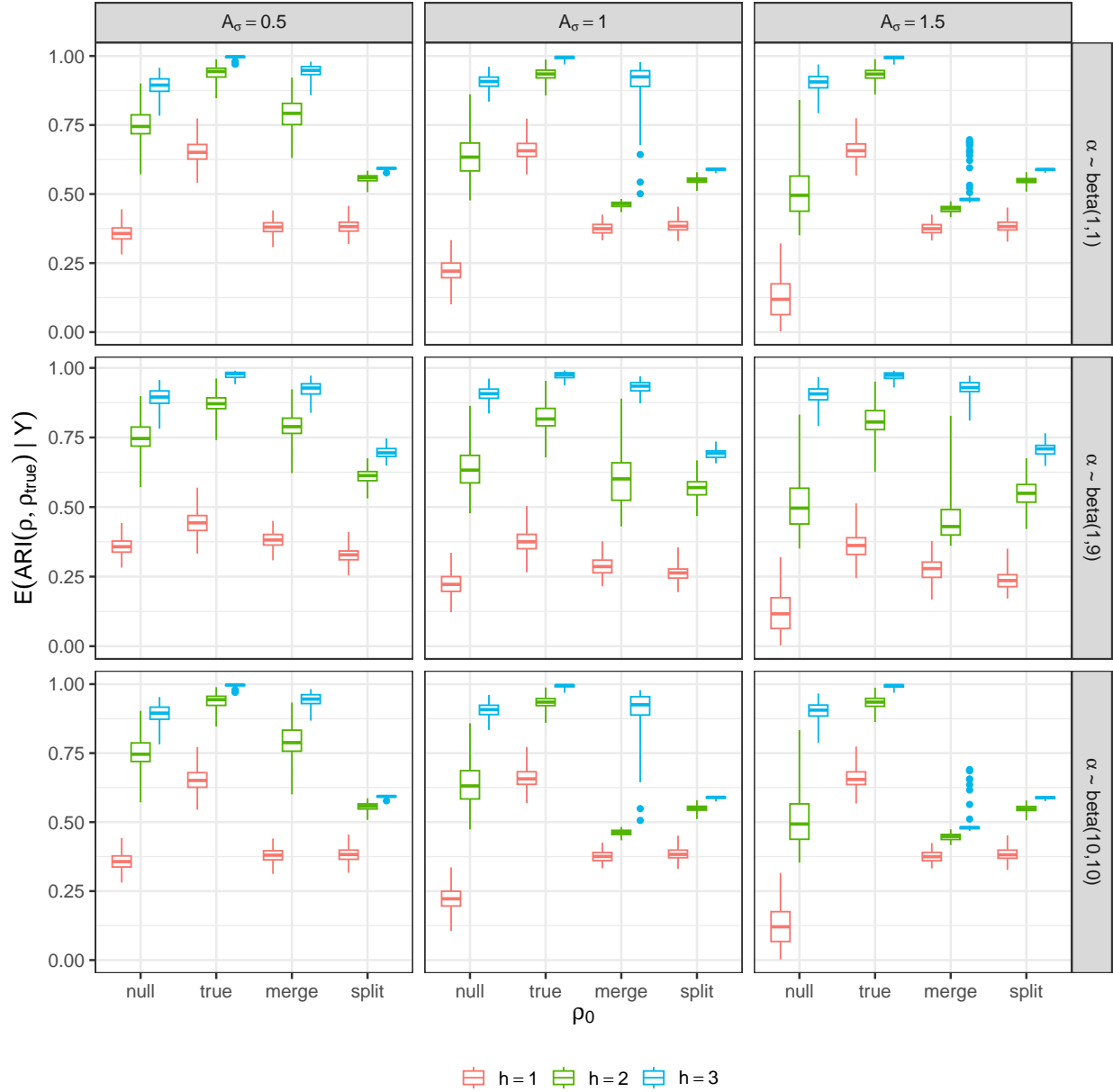
Figure S.4: Results for unit local random α. Distribution of $E(ARI(\rho, \rho_{true}) \mid \boldsymbol{Y})$ for different choices of ρ_0 (x-axis) across 100 replicated data sets using different values for the cluster means separation (boxplot colors). Each panel shows results for different combinations of prior choices for α and A_σ. Here $\rho_0 =$ null corresponds to a model that does not include an initial partition. Notice that when $\rho_0 =$ null results do not change for different values of α, as that parameter is not included in the model.
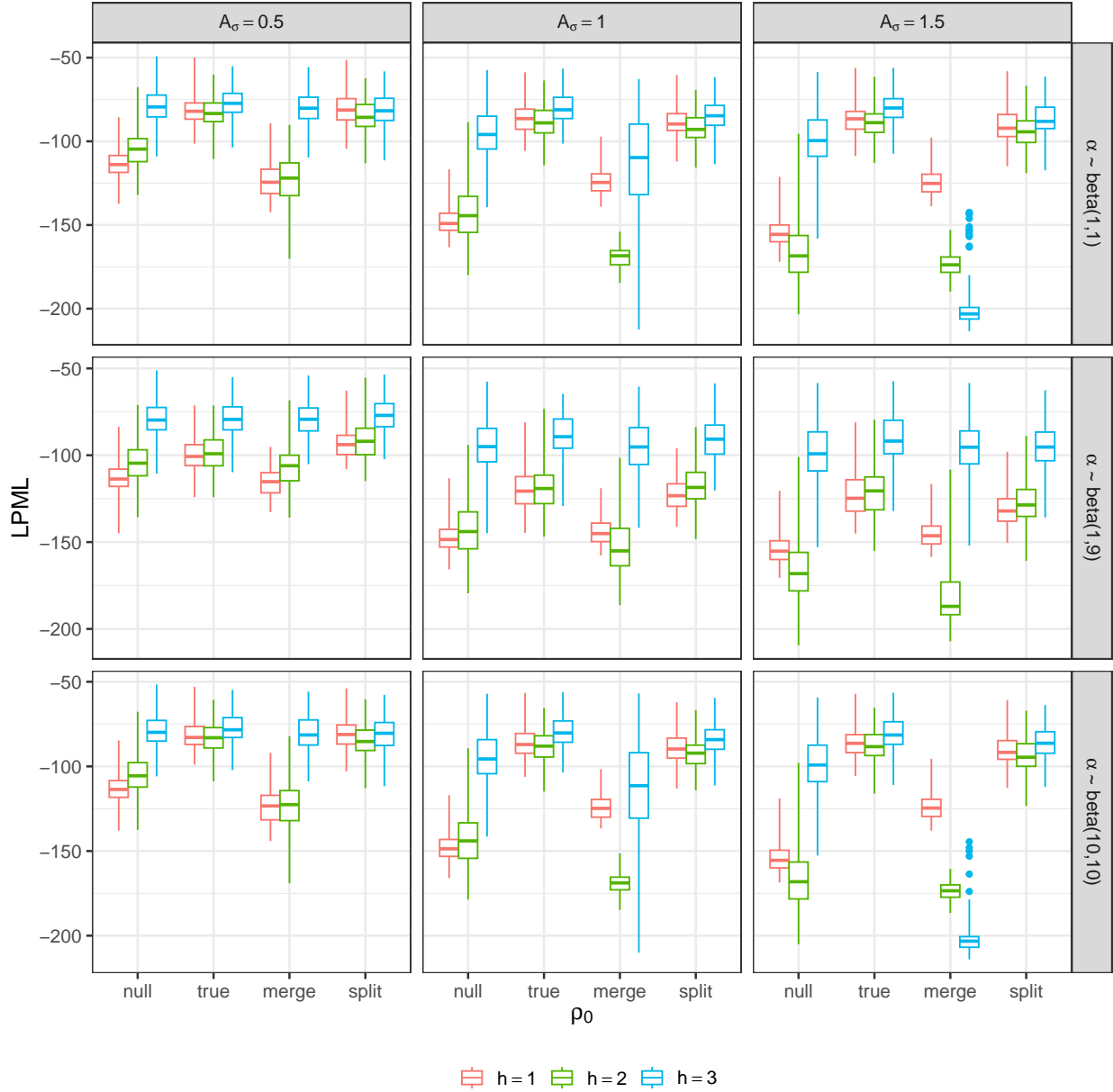
Figure S.5: Results for unit local α. Distribution of LPML for different choices of ρ_0 (x-axis) across 100 replicated data sets using different values for the cluster means separation (boxplot colors). Larger values of LPML indicate a better fit. Each panel shows results for different combinations of prior choices for α and A_σ. Here $\rho_0 = $ null corresponds to a model that does not include an initial partition. Notice that when $\rho_0 = $ null results do not change for different values of α, as that parameter is not included in the model.

In addition to the two initial partitions employed in the simulation study of Section 3.3 of the main document, we also considered those in the second and third rows of Figure S.1. Figures S.6 and S.7 show the corresponding results. It seems that generally speaking,

splitting clusters with similar response values tends to produce worse partition estimates than those that merge units whose response values are quite different. And these trends seem to hold even for the unit local model.
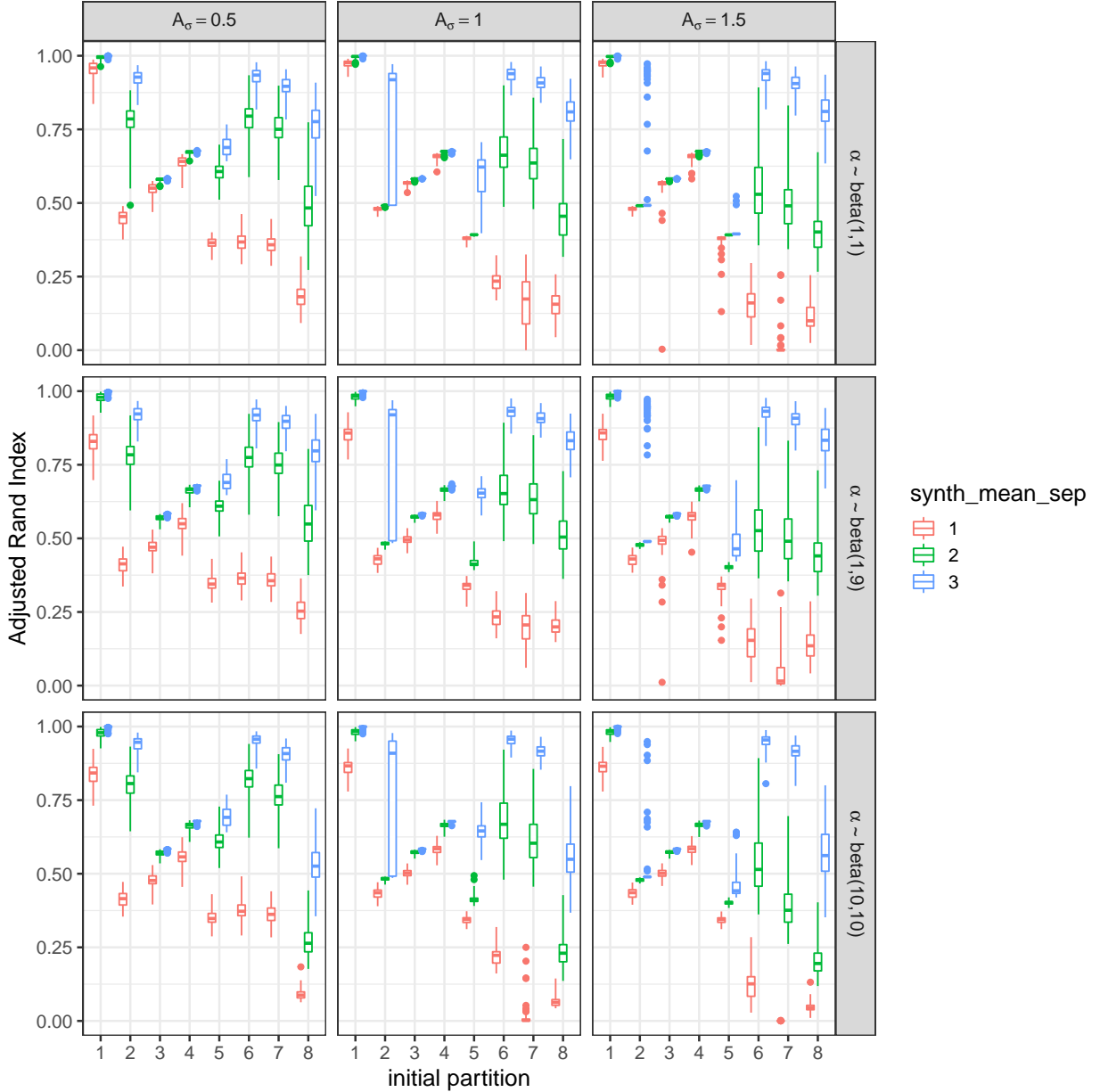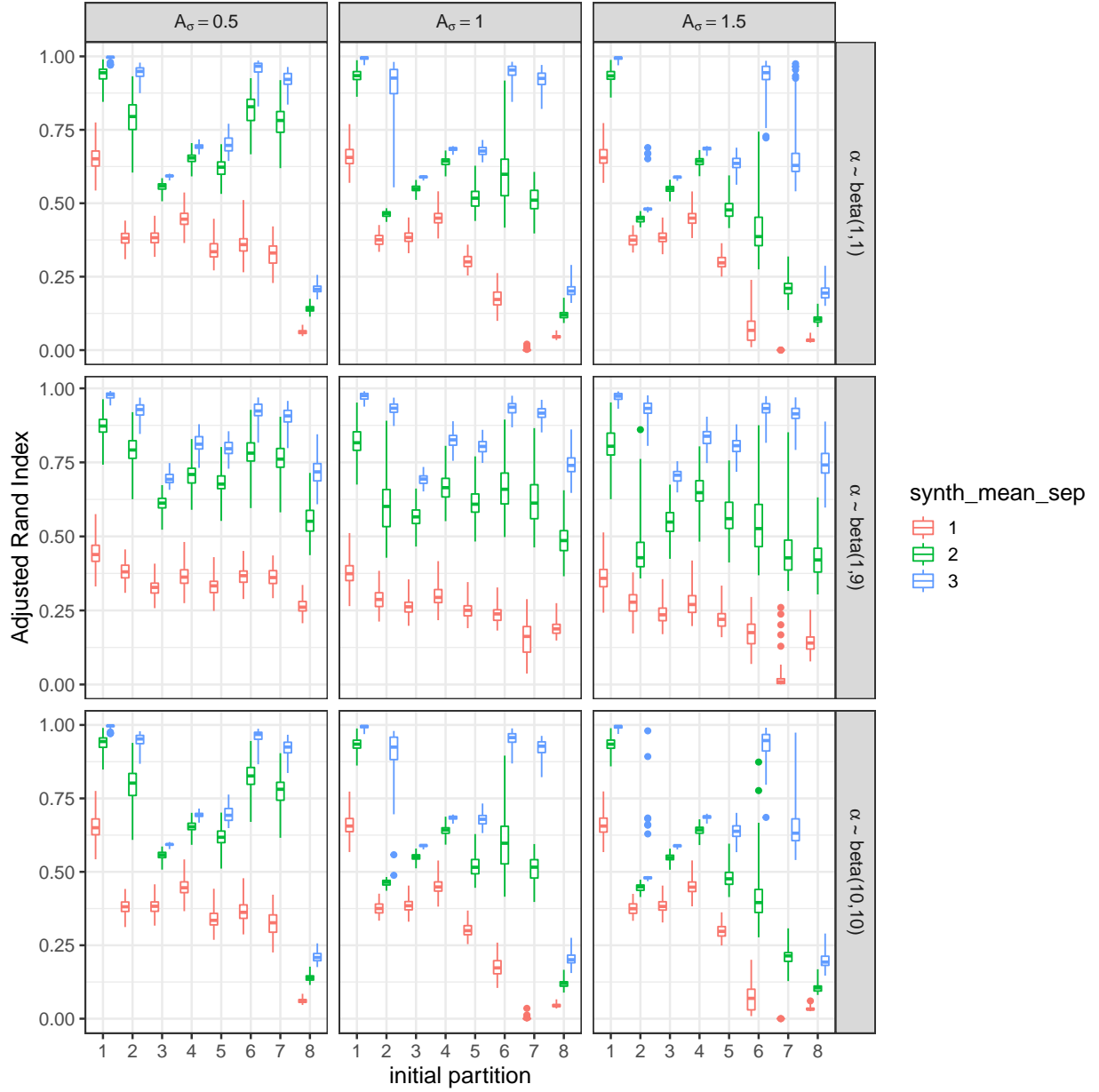

Figure S.6: Results for global α using all 8 initial partitions (x-axis) across 100 replicated data sets using different values for the cluster means separation (boxplot colors). Larger values of ARI indicate a better estimate of the partition. Each panel shows results for different combinations of prior choices for α and A_σ. Here $\rho_0 =$ null corresponds to a model that does not include an initial partition.

Figure S.7: Results for unit local α using all 8 initial partitions (x-axis) across 100 replicated data sets using different values for the cluster means separation (boxplot colors). Larger values of ARI indicate a better estimate of the partition. Each panel shows results for different combinations of prior choices for α and A_σ. Here ρ_0 = null corresponds to a model that does not include an initial partition.

S.2 Simulation with a Locally Weighted Prior Partition

In this very small simulation, we explore the performance of the method when some units *a priori* cluster with high probability and the case when some units *a priori* belong to different clusters with high probability. It may be the case that there exists more prior uncertainty associated with particular sections of the initial partition than with others. This can easily be incorporated in the prior construction by way of the unit specific beta prior distributions. In particular, for one partition we have $\alpha_i \sim \text{Beta}(a_i, b_i)$ so that particular subsections of the partition are maintained unless the data strongly contradict. To do this it is enough to set a_i and b_i so that the probability of reallocating is small (e.g., $a_i = 1$, $b_i = 10$). To illustrate this consider Figures S.8 and S.9. Figure S.8 displays a synthetic dataset of 100 observations in which there are two clusters one centered at -1 and the other at 1. The top plot in Figure S.8 displays the initial partition employed. Notice that the initial partition is such that the two clusters are split and there are five observations on the edge shared by both clusters (the "+" points) that are assigned in the initial partition to their own cluster. The bottom four plots in Figure S.8 are different fits of model with different combinations of A (the upper bound on on σ_i) and M (the scale parameter of the CRP). Notice that a section of the initial partition that splits the two main clusters is overridden by the data, but the prior assigned to the "+" points is such that it forces those points to remain in their own clusters.

Next, consider Figure S.9. The data generating proceedure is similar to that of Figure S.8. Now however, the initial partition contains a group of five units that clearly should not be in the same cluster based on their response value (the "+" points). Notice here that for specific hyper-prior values these points too are able to remain in the same cluster, but they are absorbed by one of the two bigger clusters. As a result, it is possible to essentially fix part of the initial partition if the users have enough prior information to warrant it.

S.2.1 Prior simulations

Figure S.10 displays the prior partition probabilities where $\rho_0 = \{\{1, 2\}, \{3, 4, 5\}\}$ is the initial partition with cluster specific α values. This provides the user quite a bit of control on how to weight the initial partition.

S.2.2 Posterior simulations

Figures S.11 and S.12 show the distribution of the WAIC and LPML across simulations for the different models. We can observe similar patterns for the Informed Partition Model and the Centered Partition Process. The best fit is obtained when the models are informed using ρ_{true}, while the worst fit is obtained when the initial partition is ρ_{merge}. Results under ρ_{split} an initial partition are comparable ρ_{true}; even if the partition is not the correct one the units are still informed towards coherent groups, as ρ_{split} divides each of the 4 clusters of the
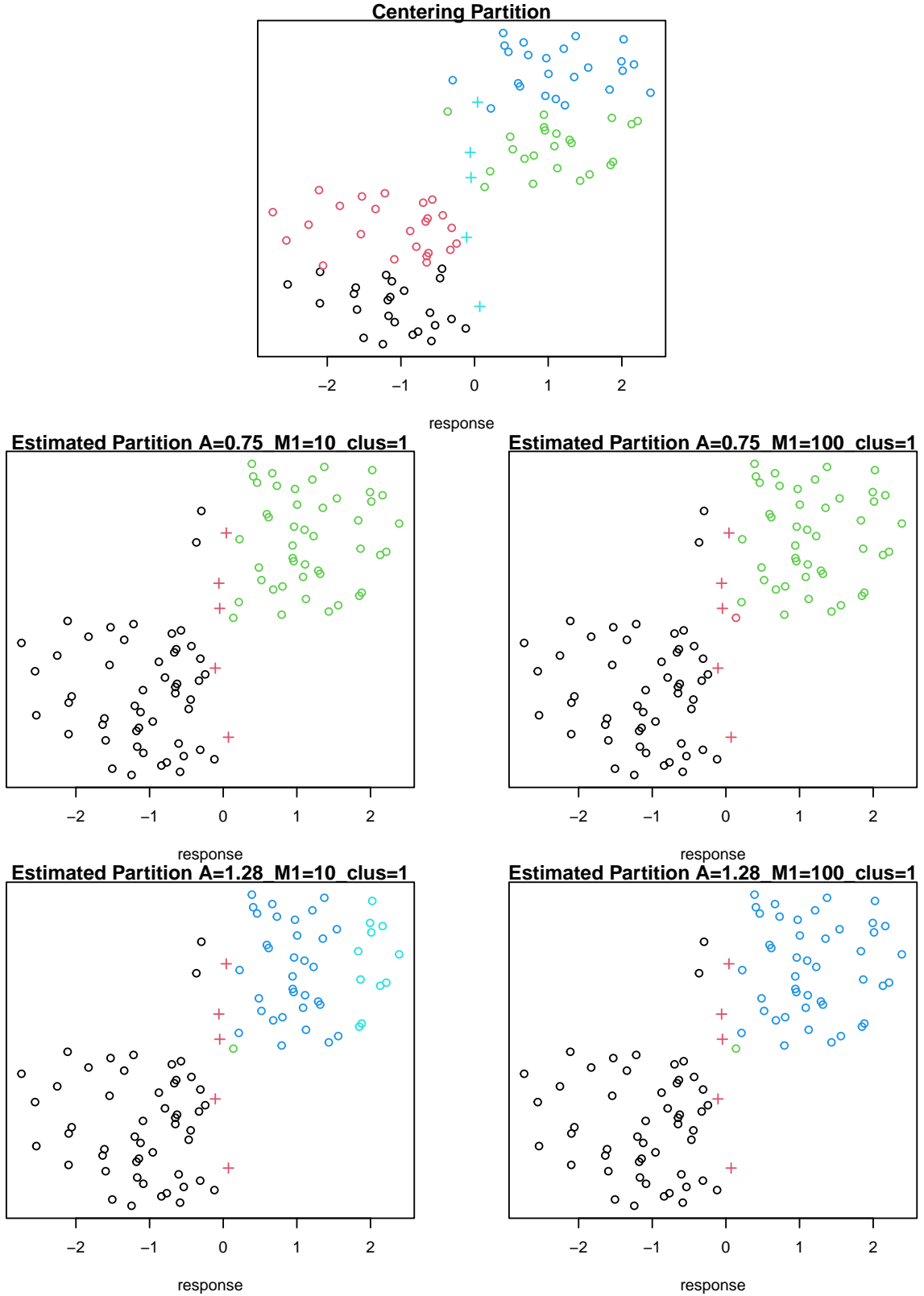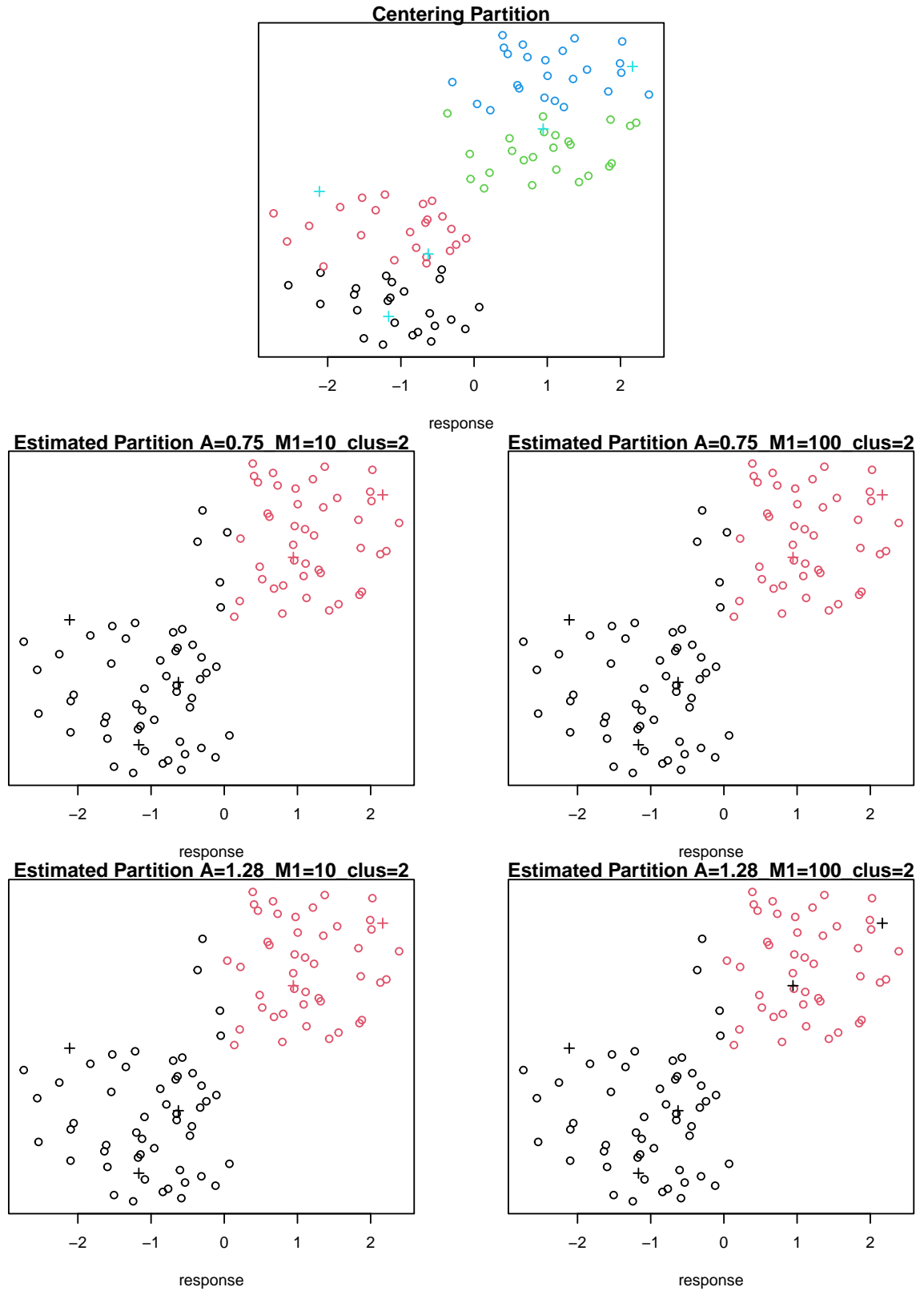
Figure S.8: Results from a small simulation study that explores the impact that the prior on α_i has on posterior partition estimate. The prior employed was such that α_i for the "+" points were not reallocated and as a result they stayed in their own cluster, even though the rest of the initial partition was overridden.

Figure S.9: Results from a small simulation study that explores the impact that the prior on α_i has on posterior partition estimate. The prior employed was such that α_i for the "+" points were not reallocated.
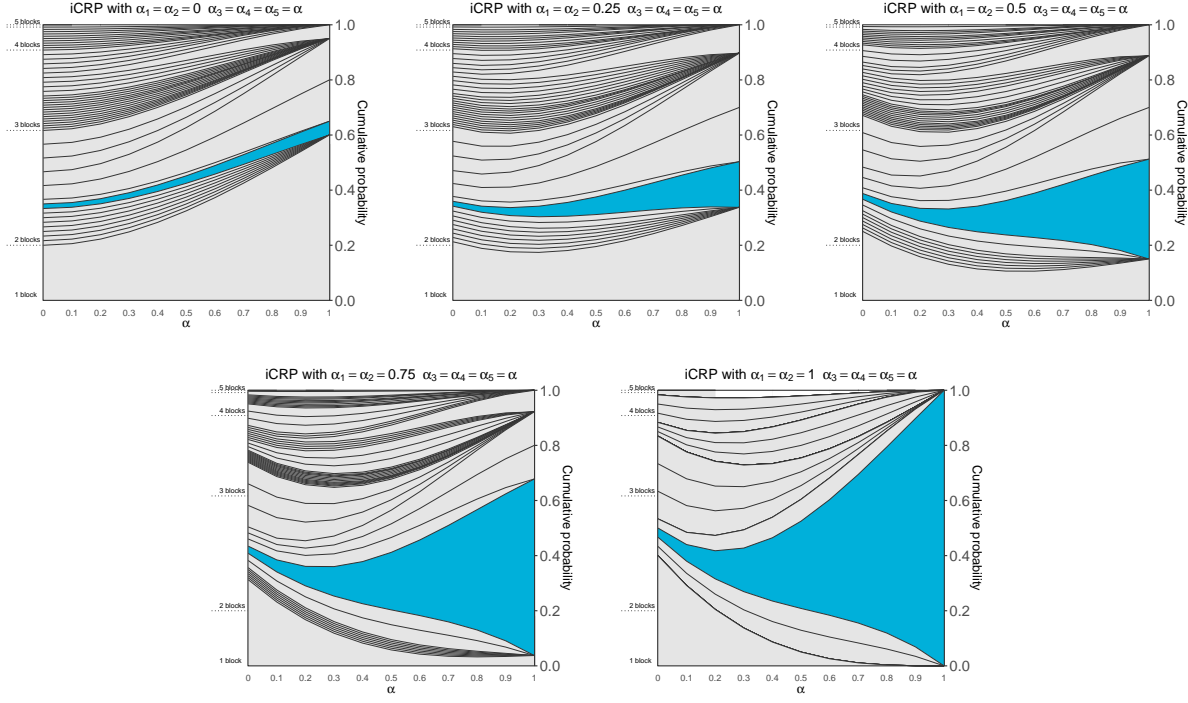
50

Figure S.10: Prior probabilities for each of the 52 partitions when the prior guess is $\rho_0 = \{1,2\}\{3,4,5\}$ (highlighted in blue) for different specifications of the informed partition model using the CRP prior (iCRP). The cumulative probabilities across different values of the penalization parameters are joined to form the curves, while the probability of a given partition corresponds to the area between the curves.

simulation in two. The LSP prior behaves differently as it seems to show a good fit overall. However, figures in Section 3.2 show that this prior tends to induce a small inflation in the prior probability for the initial partition unless the tuning parameter is really small.
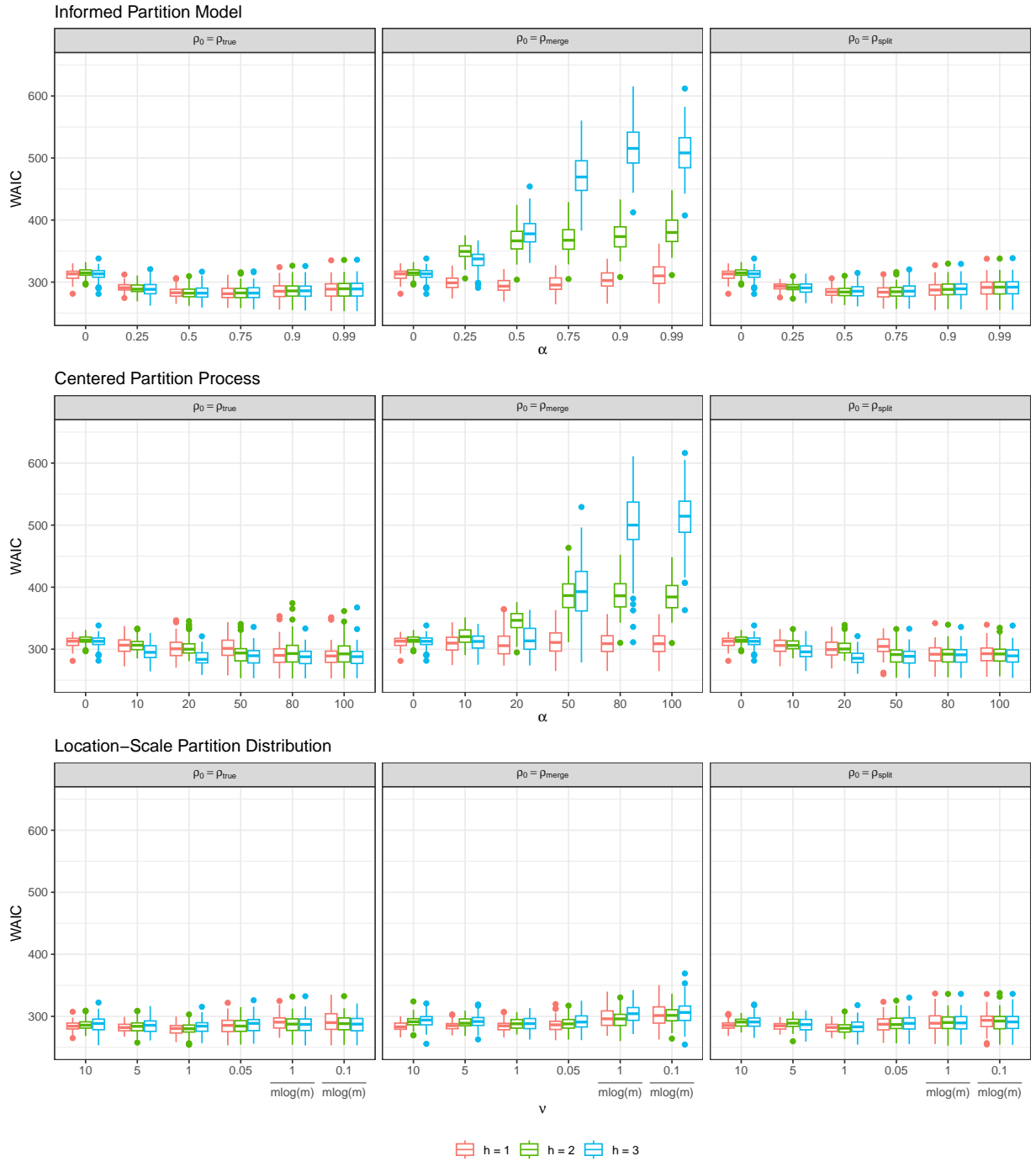
Figure S.11: Comparison of posterior results using the iCRP, CPP, and LSP priors for different values of their tuning parameters. Each boxplot represents the distribution of WAIC across the 100 generated data sets, with colors distinguishing between data-generating scenarios. Notice that the values of the tuning parameters are not directly comparable.
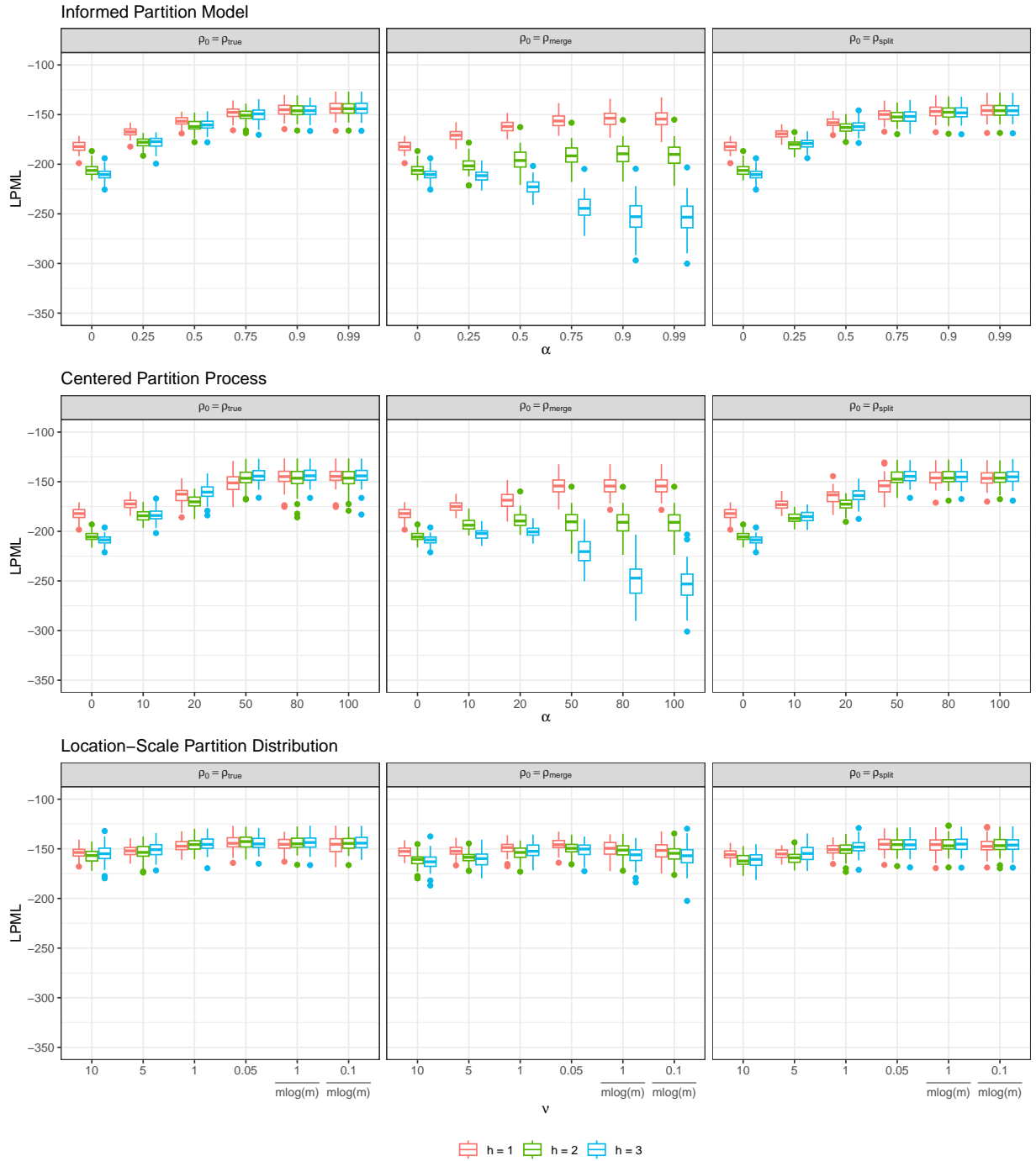
Figure S.12: Comparison of posterior results using the iCRP, CPP, and LSP priors for different values of their tuning parameters. Each boxplot represents the distribution of LPML across the 100 generated data sets, with colors distinguishing between data-generating scenarios. Notice that the values of the tuning parameters are not directly comparable.